Thesis Submitted to the School of Chemical and Physical Science

Faculty of Science and Engineering

Flinders University

Master Thesis

November 2017

Investigating the Structure of Self-Assembled Monolayers

Related to Biological Cell Membranes

Ahlam Rayan Alharbi

Supervised by:

Prof. Gunther Andersson

A/Prof. Ingo Koper

Declaration

I hereby declare that this thesis is my own work and does not incorporate any previous submitted work for Flinders University or any other University. There are some contributions in this work from several literatures but all of them have been referenced to their original sources. This work has been performed under the supervision of Prof. Gunther Andersson & A/Prof. Ingo Koper.

Ahlam Rayan Alharbi

08th of November 2017

Acknowledgment

Abstract

Tethered bilayer lipid membranes (tBLMs) are solid supported membranes, where the solid supported substrate is separated from the artificial lipid bilayer by an anchorlipid such as 2, 3-di-O-phytanyl-glycerol-1-tetraethylene glycol-D,L-lipoic acid ester lipid (DPTL or DPhyTL). Tethered bilayer lipid membranes are based on self-assembled monolayers (SAMs) of anchorlipids. The chemical structure of the tether-segment of the anchorlipids has a significant effect on the properties of the artificial Tethered bilayer lipid membranes such as its fluidity. Therefore, this study focuses on examining the thickness, elemental composition and orientation of DPTL SAMs as well as SAMs of a dilution of 0.16 mg/ml of DPTL with 0.04 mg/ml of mercaptoethanol (ME). The length measurements of the SAMs were obtained from applying neutral impact collision ion scattering spectroscopy (NICISS). The estimated length of the DPTL SAMs was 3.9 nm whereas the estimated thickness of the diluted SAMs of DPTL was 1 nm. X-ray photoelectron spectroscopy (XPS) was applied to the investigated SAMs in order to determine their elemental composition and chemical state of elements. Both SAMs of DPTL and a diluted DPTL composed of four core elements as appeared from XPS measurements Gold4f, Oxygen1s, Carbon1s and Sulphur2p with different relative intensities of elements. The orientation of the molecules forming the monolayer has been examined by means of metastable induced electron spectroscopy (MIES). DPTL SAMs are standing up in a very oriented way and a methyl group are dominating the surface whereas the diluted DPTL SAMs are lying flat and a methylene group are dominating the surface. Additionally, in this study, a case study of two types of SAMs of organic films 11-Mercaptoundecanoic acid (11-MUA) & 1-Dodecanethiol (DDT) have been structurally examined by means of NICISS, XPS and MIES. The investigation of the organic films have been performed due to their simple structure. The SAMs of 11-MUA and DDT have been investigated as preliminary study before analysing the structure of the SAMs formed by the anchorlipids.

Table of Contents

List of figures

List of tables

Abbreviations

NICISS	Neutral Impact Collision Ion Scattering Spectroscopy.
XPS	X-ray Photoelectron Spectroscopy.
MIES	Metastable Induced Electron Spectroscopy.
UHV	Ultra-High Vacuum.
SAMs	Self-Assembled Monolayers.
sBLMs	Solid Supported Bilayer Lipid Membranes.
tBLMs	tethered Bilayer Lipid Membranes.
DPTL or DPhyTL	2, 3-di-O-phytanyl-glycerol-1-tetraethylene glycol-D,L-lipoic acid ester lipid.
ME	2-Mercaptoethanol.
11-MUA	11-Mercaptoundecanoic Acid.
DDT or 1-DDT	1-Dodecanethiol.
TOF	Time of Flight.
NR	Neutron Reflectivity.
SPR	Surface Plasmon Resonance.
SVD	Singular Value Decomposition.
KE	Kinetic Energy of photoelectron.
BE	Binding Energy of photoelectron.
eV	Electron Volt.
KeV	Kilo Electron Volt.
hv	Excitation photon energy.
Mg	Magnesium.

Au	Gold element.
Si	Silicon.
Ti	Titanium.
Cr	Chromium.
CPS	Count per Second.
Φ	Work function.
Φsp	Spectrometer work function of the detector.
Δ	Band gap.
ARXPS	Angle-Resolved X-ray Photoelectron Spectroscopy.
Si	The measured spectra.
S_n^r	The reference spectra.
a_n	The weighting coefficients.
Å	Angstrom.

1 Introduction

1.1 Basic concepts of Biological cell membranes
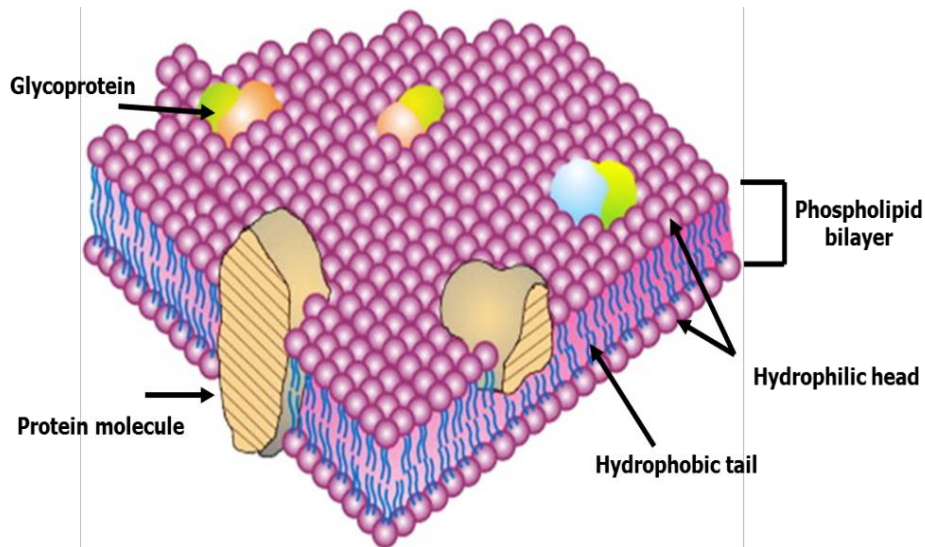
Figure 1: *Schematic representation of the first proposed structure, in 1972, of the Fluid Mosaic Cell Membrane* [1, 2].

It is a well-known fact that cells are the essential units of all living organisms. Therefore, understanding the structure of cells creates the potential of developing treatments for diseases as bacteria and viruses have a direct interaction with cell membranes. That means the cell membrane is significant to the cells survival. Cell membranes are continuous fluid lipid bilayer membranes that play a significant role in cell structure as they surround the cell. Cell membranes protect cells and host many types of proteins which are very essential to many processes of cell functions (e.g. cell division, signal transduction, metabolic waste disposal etc.) occur at the cell membrane [3, 4]. The lipid bilayer membrane is a biological fluid mosaic cell membrane that acts as a protector of the intracellular components of the cell from the outside environment and its surroundings [5] (**fig 1**). The cell membrane also acts as a selective filter that has the ability to regulate the movement of the substances from inside the cell to the outside of the cell and vice versa in a molecular level. Biological cell membranes consist of two major lipids which are Phospholipids and Cholesterol [3, 6]. Most of the lipids in bio-membrane are phospholipids that consist of a stable arrangement of amphiphilic lipids that have hydrophobic and hydrophilic components. As **fig 2** illustrates, the hydrophobic tails are non-polar tails that consist of a couple of alkyl (hydrocarbon) chains whereas the hydrophilic head groups are polar groups that consist of choline and glycerol that is attached to phosphate groups. Head groups are linked to alkyl chains via ester linkages [7]. In additional to these main components, as **fig 1** illustrates, natural bio-membranes have more than hundred

components (e.g. receptors, ion channels and carbohydrates etc.) that actually hinder scientists from studying and investigating the structure of these membranes [8, 9]. Therefore, it was necessary to artificially create and synthesised cell membranes that mimic the structure of the major component forming the natural biological cell membrane. Phospholipids are fats that form the majority of the cell membrane and they are defined the most significant feature of biological cell membranes (**fig 2**).
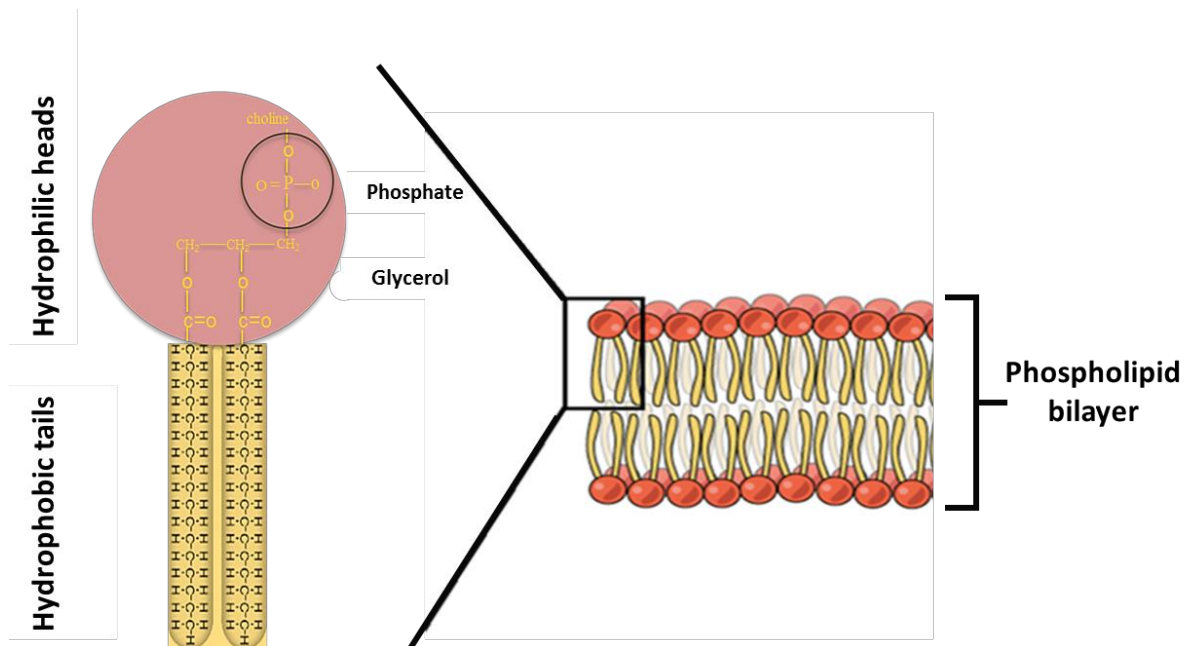
Figure 2*: This diagram displays the Phospholipids (amphipathic molecules) structure. Phospholipids consist of hydrophobic section & hydrophilic section* [10].

1.2 Model systems of bio-membranes

The complexity of natural bio-membranes hinders scientists from investigating the structure of these membranes. Therefore, plenty of model systems of natural biological membranes have been artificially synthesized in order to simplify the natural complexity of natural bio-membranes [6]. These artificial cell membrane systems resemble some of the fundamental chemical and physical characteristics of the natural bio-membranes (e.g. membrane fluidity and membrane electrical resistance) [9, 11]. That means, only a few types of lipids are used in the formation of a model membrane that would help in examining biophysical and thermodynamic properties of a certain type of lipids in cell membrane. The development of artificial cell membranes helps in studying cellular processes (e.g. ions transfer) and exploiting the nature of cellular processes such as cell signalling for biotechnological applications such as cell and tissue culture technologies [4, 12]. Artificial cell membrane systems are lipid molecules that have the ability of spontaneous self-organization

in the presence of an aqueous medium. Several types of model systems of natural biological membranes have been developed (**fig 3**). Among these artificial cell membranes, solid supported bilayer lipid membranes (sBLMs) have attracted a great deal of attention due to their relative stability as well as their allowance of being characterized and analysed via using several types of surface analytical techniques (e.g. atomic force microscopy AFM) in comparison to other free standing bilayers. Solid supported bilayer lipid membrane is phospholipid bilayer placed on a solid surface. As an extension of solid supported bilayer lipid membrane, tethered bilayer lipid membranes (tBLMs) have been synthesised with a tethering molecules that separate the surface from the bilayer lipid membrane [6, 11].
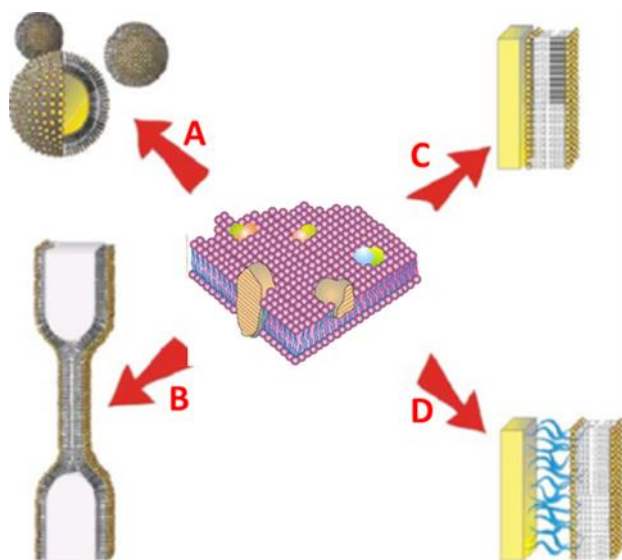
Figure 3: *Illustrates the four model systems for a natural biological cell membrane (centre).* ***A)*** *Vesicles*. ***B)*** *Bilayer lipid membranes*. ***C)*** *Solid supported membranes*. ***D)*** *Tethered bilayer lipid membrane* [13].

1.3   Tethered bilayer lipid membranes (tBLMs)

Tethered bilayer lipid membranes (tBLMs) is the last synthesized and modified version of artificial cell membranes [6, 14]. Solid supported bilayer lipid membranes are separated from the phospholipids bilayer only by a thin layer of water (10-20 Å) [15] in thickness whereas in tBLMs, the phospholipid bilayers are covalently attached to a gold surface through flexible, hydrophilic spacer groups. These spacer groups separate the bilayer from the substrate thus, the interaction between the membrane and the substrate is almost non-existent [16, 17]. Additionally, Spacer groups or tethered groups provide several benefits to the surface and to the function of biomaterials as they cover a small substrate roughness and provide an ion and water reservoir underneath the bilayer. Moreover, spacer groups can protect embedded biomaterials from losing their functionality due to denaturation that comes from the interaction between biomaterials and surfaces. In the formation of both sBLMs and tBLMs, the gold substrates are the most widely used substrates because they can be functionalised easily via thiol and sulphur-based anchorages [6, 15]. Additionally, Gold substrates can be employed as an electrode for plenty of surface analytical techniques that require a metallic solid support (e.g. surface plasmon resonance) [8, 18].
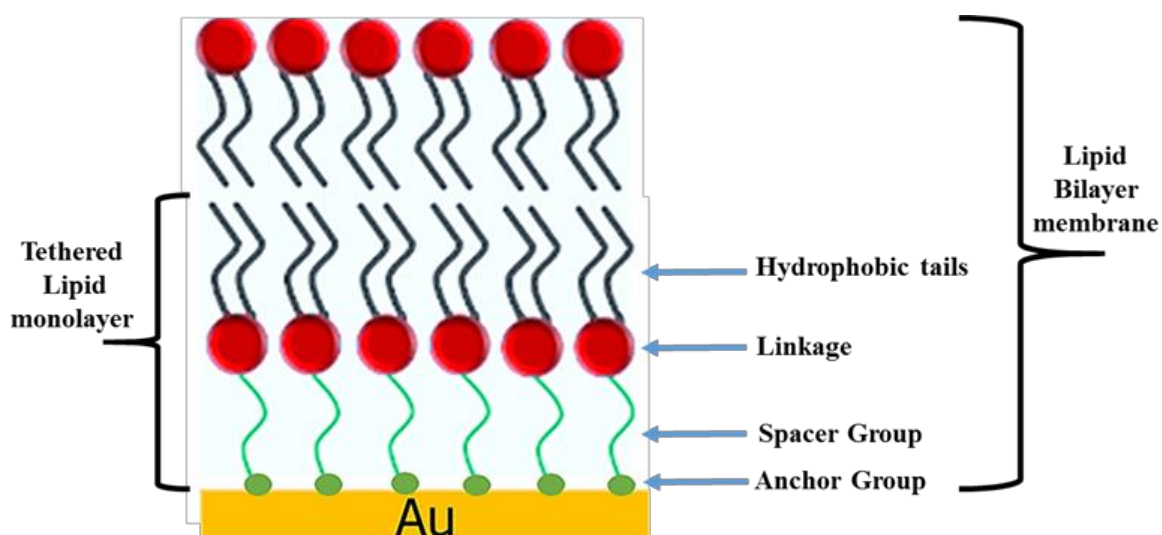
Figure 4: A basic schematic diagram of tethered lipid bilayer membranes (tBLMs) and tethered monolayer lipid membranes which consists of four distinct regions anchor groups, spacer groups, hydrophobic tails and linkage [6, 8].

Tethered lipid monolayer cell membrane (thiolipids) (as shown in **fig 4**), have four distinct parts (anchor groups, spacer groups, hydrophobic tails and linkage). Each part of the thiolipids has unique features and characteristics in the architecture of the lipid membrane. First, anchor groups (anchor units) are made of cyclic disulphide and are attached to the substrate via a covalent bond and the majority of these anchor groups are actually based on the interaction of Gold and sulphur. They are significantly helpful in terms of the stability and surface immobilization of the lipids spacer molecule on the surface [4]. The second significant component of the thiolipids is spacer groups. Spacer group is coupled to the hydrophobic tails via ether bonds because ether bonds provide more stability than the ester bonds. Spacer groups are actually hydrophilic groups consist of poly-ethylene oxide units ($C_{2n}H_{4n+2}O_{n+1}$) that serve as a polymer cushion which provide several benefits to the surface and to the biomaterials function [4]. Providing an ionic reservoir underneath the membrane and compensating for surface roughness effects are some of the benefits that the polymer cushion has for the surface. Additionally, polymer cushion protects embedded biomaterials from losing their functionality due to denaturation which comes from the interaction between biomaterials and surfaces. The third significant region in the tethered lipid monolayer cell membrane is a linkage group. Linkage group separates the hydrophobic and hydrophilic sections in the tethered lipid molecule. Finally, the hydrocarbon tails (isoprenoid tails) are phytanyl chains that improve the stability and the fluidity of the thiolipid under extreme environmental conditions such as high temperature [4, 8, 19]. There are a wide variety of tethering anchor-lipids (e.g. DPTL, DPAL, DPGL, DPSL and DPSDL) [9] that differ from

each other by their length and the components of their anchor groups. In the present work, we are interested more on 2,3-di-O-phytanyl-glycerol-1-tetraethylene glycol-D,L-lipoic acid ester lipid (DPhyTL or DPTL) tethering anchor-lipids as it is the first and the main thiolipid ever synthesised [4, 19].

1.4 DPTL Tether-Lipid

DPTL tethered lipid monolayer is an abbreviated name of 2,3-di-O-phytanyl-glycerol-1-tetraethylene glycol-D,L-lipoic acid ester lipid. In 2003 [8], DPhyTL was synthesised as a tethered bilayer lipid membrane with a formula ($C_{59}H_{117}O_8S_2$) [4]. DPhyTL which has methyl terminated group (CH_3) [20], (as represented in **fig 5**) consist of two non-polar phytanyl chains ($C_{20}H_{42}$) is covalently bounded to the spacer unit (polar tether group that consist of tetraethyleneoxy chain) via a chiral glycerol unit that has ether linkages that help in preventing hydrolytic cleaving. Finally, the polar tether group is attached to lipoic acid residue that can anchor the thiolipid to the solid support via forming two covalent bonds with
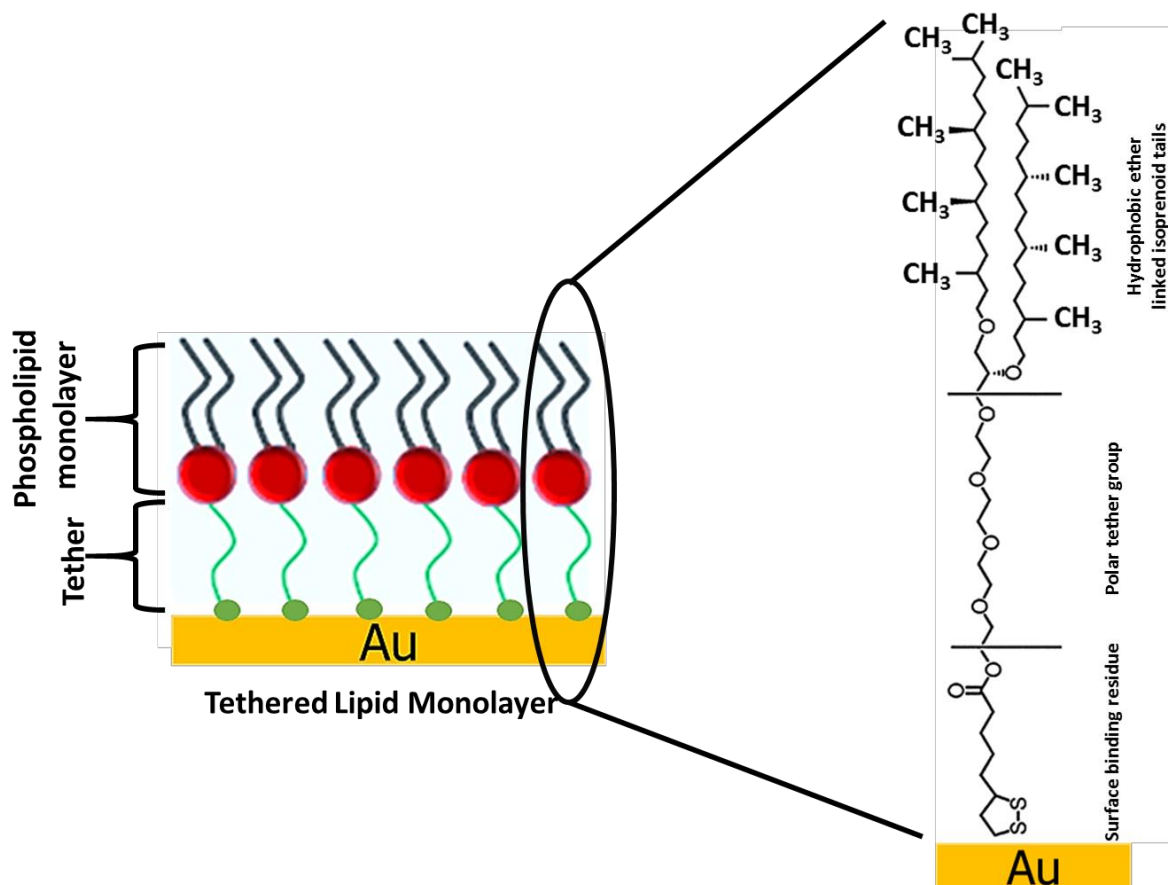
Figure 5: *This diagram schematically illustrates the chemical structure and the arrangement of the 2,3-di-O-phytanyl-glycerol-1-tetraethylene glycol-D,L-lipoic acid ester lipid (DPhyTL) molecules* [6, 14].

the surface (e.g. gold surface) [4]. The length (thickness) of the DPhyTL thiolipid has been determined theoretically by using a software called Chem3D Ultra 6.0 and it was found to be about 5nm in its fully stretched orientation [8, 11]. The investigation of molecular arrangement of the DPhyTL and other tethering anchor-lipids is a preliminary step that helps in developing the bilayer structure of the model systems of natural bio-membranes since artificial cell membranes can shed some light on understanding physical properties of biological materials. Additionally, studies of the model systems would be useful in terms of exploiting the tricks of nature for biotechnical applications (e.g. vesicles usage for drug delivery and building biosensors) as well as understanding the function and the way that the membranes usually behave [4, 8].

1.5 The Impact of the Tether Structure on Bilayer Properties

The structure of the lipid bilayer membrane can be affected by the chemical nature of the sub-membrane space. Additionally, the structure of the space underneath the bilayer has an important impact on the functional incorporation of membrane proteins [6]. Several physical parameters such as bilayer fluidity [21] bilayer impedance [13] as well as the sub-membrane space hydration [22] have been utilized to describe the architecture of various types of tethered bilayer lipid membrane. That means, in order to create a high quality bilayer lipid membrane that resemble the natural membrane, a high fluidity, a high electrical impedance and high sub-membrane hydration as well as low capacity must be achieved. These four parameters allow proteins within the membrane to function well [6] because proteins are significantly involved in some physiological processes such as cardiac function [23]. The electrical properties in tethered bilayer systems are essential for ensuring that the transportation of ions within the membrane is mainly due to the function of embedded protein whereas the sub-membrane hydration is significant for allowing protein to function. Studies have shown that the sub-membrane space in tethered bilayer lipid membrane is controlled by the structure of the spacer region that separates the lipid bilayer from the solid support [6, 9].

In regards to DPTL tethered lipid monolayer, studies have illustrated that even though the spacer groups in DPTL monolayers consist of polyethylene glycol units which known to be water-soluble, they are poorly hydrated [9]. Additionally, the tethered bilayer lipid membrane fluidity is decreased when they are synthesized with DPTL molecules as a result of a high capacity which play a significant role in minimizing the velocity of the membrane [6]. That means, DPTL monolayers need to have a less packing density, a high velocity and a high sub-

membrane hydration in order to make a high quality artificial bilayer lipid membrane. According to some studies [9], one possible approach that helps to decrease the anchorlipid density (e.g. DPTL density) is a dilution of DPTL self-assembled monolayers with a shorter surface-active backfilling molecules such as mercaptoethanol (ME) [9] which is a chemical component with a chemical structure of (C_2H_6SO). As ME has sulphur as an anchor group, which has a high affinity for gold surfaces, it would bind to the gold substrate and create rooms among the spacer group segments [6, 24]. This space then would increase the sub-membrane hydration as well as decrease the density of the membrane.

1.6 Previous studies of DPhyTL thickness

Several values of the length of the DPhyTL thiolipid self-assembled monolayers have been obtained experimentally from different studies by means of different analytical techniques. Investigation and studying the length of self-assembled monolayers is significant in terms of understanding the relation between the functionality and the substrate structure, specifically the property of the electron transformation in the membrane [25, 26]. SPR spectroscopy is a surface-sensitive technique used for measuring the optical thickness of ultra-thin films that get adsorbed by metals substrates, such as thiolipid monolayers [27]. In Surface Plasmon Resonance (SPR) studies, researchers have immersed the ultra-flat gold substrate into an ethanolic solution containing 0.2 mg/ml of lipids for an hour. The thickness of DPhyTL monolayer was measured to be 3.2 ± 0.2 nm [8]. In another study, the investigation of the length of DPhyTL monolayer was determined via a specific analytical technique known as Neutron Reflectivity (NR). NR is an ideal tool that is used in order to examine buried interfaces which would help in determining the structure of thiolipids. In NR measurements, the monolayer was formed by using the commonly used procedure of forming the monolayers (0.2 mg of lipids/ml of ethanol) for 24 hours and its thickness was approximately 3.9 nm [3, 4] as shown in **table 1**.

Table 1. This table illustrates the thickness values of DPTL monolayers that have been measured via using two different analytical techniques (SPR and NR) as well as the theoretical thickness values of the DPTL monolayers [3, 8].

	Theoretical (calculated) thickness	Thickness with SPR	Thickness with NR
DPTL SAMs Thickness (nm)	5	3.2 ± 0.2	~ 3.9

1.7 11-MUA and DDT alkanethiols

Organic films such as 11-Mercaptoundecanoic Acid and 1-Dodecanethiol are essential agents for changing features of substrates. Therefore, they have many applications in the fields of biology, optics and coatings [28]. Self-assembling of alkanethiols molecules (e.g.11-MUA and DDT) with different terminal groups were also of an interest in the present study in terms of understanding how the chain type influences the structure (thickness and orientation) with a layer attached to the substrate. As **table 2** illustrates, 1-Dodecanethiol and 11-Mercaptoundecanoic acid alkanethiols have the same backbone but with different end groups. DDT ends with methyl (CH_3) whereas 11-MUA has

Table 2: This table displays the chemical structure and the formula of self-assembled monolayers of two types of alkanethiols with different terminal groups that are performed on gold substrates [19, 28] and [29].

	11-MUA	DDT
Formula	$C_{11}H_{22}O_2S$	$C_{12}H_{26}S$
Theoretical Length (nm)	1.53	~1.5
Chemical Structure	COOH ... SH Au 11-MUA	CH_3 ... SH Au DDT

carboxyl (COOH) terminated thiol [29]. The commonly utilized method for the formation of self-assembled monolayers of DPhyTL molecules and alkanethiols is immersing gold substrates in an ethanol-lipid solution to a concentration of 0.2 mg/ml. Then the slides were thoroughly rinsed in ethanol and dried with nitrogen. Self-assembled monolayers have become the focus of deep studying and examination because they able to give a means of defining the chemical composition of surfaces and the overall structure of surfaces [25]. Some of The possible applications of SAMs of organic films (alkanethiols) on metal surfaces range from nanotechnology to fundamental surface science. SAMs of thiols can be utilized for pattern formation, corrosion prevention, as well as adjustment of wetting and wear properties of solid surfaces that can be used for developing electronics nano-devices for pattern formation [30].

2 Research Aims

The original aim of this work was examining the structure of SAMs of DPTL in a vacuum chamber when solvent molecules are involved via using NICISS. However, this aim could not be achieved due to a malfunction of the instrument and also due to the various work that need to be performed before moving to the next step which is the investigation in the presence of a liquid. Therefore, the primary aim of this work is analysing the structure (e.g. thickness, orientation and elemental composition) of SAMs of DPTL tethered lipid monolayer and compare it with diluted DPTL with mercaptoethanol molecules in a certain weight concentration. The investigation of the diluted DPTL SAMs would be helpful for upcoming studies on artificial cell membranes. In this work, several surface analytical techniques were applied such as NICISS, MIES and XPS. To achieve this goal, a case study of SAMs of two different types of alkanethiols (11-MUA and DDT) has been performed as they have simpler forms than DPTL thiols. Analysing the structure (e.g. thickness, orientation and elemental composition) of SAMs of 11-MUA and DDT would guide us to a procedure that we can rely on in analysing DPhyTL SAMs.

3   Chapter 1: Experimental details

In this project, different types of monolayers have been self-assembled in order to be investigated. They are 1-dodecanethiol (DDT), 11-mercaptoundecanoic acid (11-MUA) and a type of tethered monolayer lipid membranes known as 2,3-di-O-phytanyl-glycerol-1-tetraethylene glycol-D,L-lipoic acid ester lipid (DPhyTL). Additionally, a diluted DPTL self-assembled monolayers have also been investigated in this study as well.

3.1   Sample preparation

In this work, the used substrates were polished silicon wafers in a size of 1cm x 1cm to fit the experimental set up. These samples were cleaned with a basic piranha solution (1:1:5 H_2O_2/NH_3/H_2O solution) before they were coated with gold layer. After that, SAMs of thiols were formed for maximum 24 hours of the immersion time.

3.1.1   Substrate cleanliness

Substrate is the physical object that is used in order to support the self-assembled monolayers (SAMs). Smooth and flat substrates are essential for the formation of a high quality SAMs [8]. The used substrate is P-type polished silicon (100) wafers with a thickness of 0.525 mm and a resistivity range between 0.001-0.005 Ω.cm. The size of the silicon slides is 1cm x 1cm. Cleaned environment and materials are very significant for preparing high quality self-assembled monolayers. Therefore, silicon wafers were prepared and cleaned very well with basic piranha solution (mixture of 50 ml of milli-Q, 10 ml of hydrogen peroxide (H_2O_2) and 10 ml of ammonia (NH_3) and heated up to 70C° for an hour [31]. Then they were rinsed with distilled water, ethanol and finally dried under a nitrogen stream. The cleaning process, with a basic piranha solution, is used to remove organic contaminations and organic particles as well as increase the coverage of OH groups on the Si wafers' surfaces [8, 31].

3.1.2   Gold Deposition

In gold deposition method, the used instrument is known Q300T-D Dual Target Sputter Coater. Gold forms good self-assembled monolayers because it can bind to thiols with a reasonable strength and high affinity without making any unusual reactions with thiols. However, before depositing the gold layer, silicon slides must be adhered with chromium (Cr) or titanium (Ti) layer underneath the gold layer. The adhesion of Cr and Ti thin layer is important because it promotes the formation of self-assembled monolayers by preventing the gold layers from getting rubbed off the surface because there is a crystal lattice mismatch result in very low adhesion between gold layers directly deposited on silicon [31, 32]. Therefore,

cleaned silicon wafers were coated with 5nm of a primer (e.g. chromium or titanium) followed by 20 nm of gold (**fig 6**).

3.1.3 Preparation of Self-Assembled Monolayers (SAMs)

(a)   **(b)**   **(c)**

A- A cleaned silicon slide (1cm x1cm)

B- Silicon slide coated with 5nm of either chromium or titanium

C- Silicon slide coated with 5nm of Cr or Ti followed by 20 nm of gold
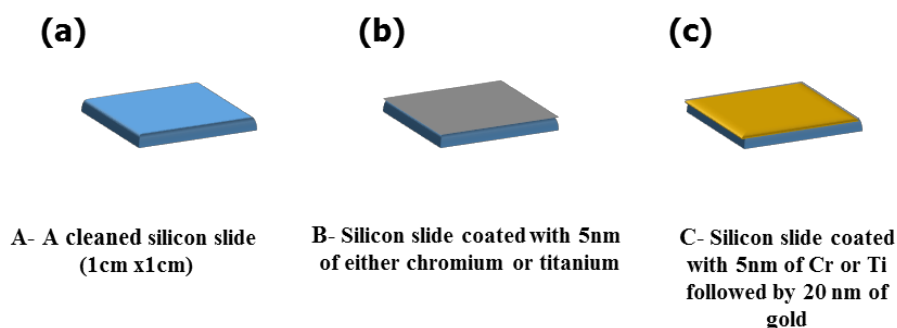
Figure 6: Gold deposition stages on silicon wafer slides.

The term "self-assembly" refers to a spontaneous molecular arrangement self-assembled on a solid substrate without any external interference [33]. In this work, self-assembled monolayers were prepared by one type of thiolipids, which is DPhyTL and two alkanethiols, which are 1- DDT & 11-MUA. The procedure of forming the monolayers that is widely used is the immersion of a cleaned ultra-flat gold substrate into a diluted solution of an absolute ethanol solution containing 0.2 mg/ml of lipids [11, 34]. Therefore, immediately after the gold layer deposition, Si slides were immersed into the ethanol solution.

In terms of the dilution of DPTL with ME, 0.16mg/ml of DPTL has been diluted with 0.04mg/ml of mercaptoethanol molecules then they self-assembled in different immersion

(a)   **(b)**   **(c)**

A- Preparing a dilution of an ethanolic solution containing 0.2 mg/ml of lipid.

B- Immersing gold-coated slides into the ethanolic solution for a desired period of time (18-24hr for a completed SAMs)

C- schematic of thiolipid. The formation of SAMs is accomplished. The monolayer is attached to the gold substrate through a spacer group.
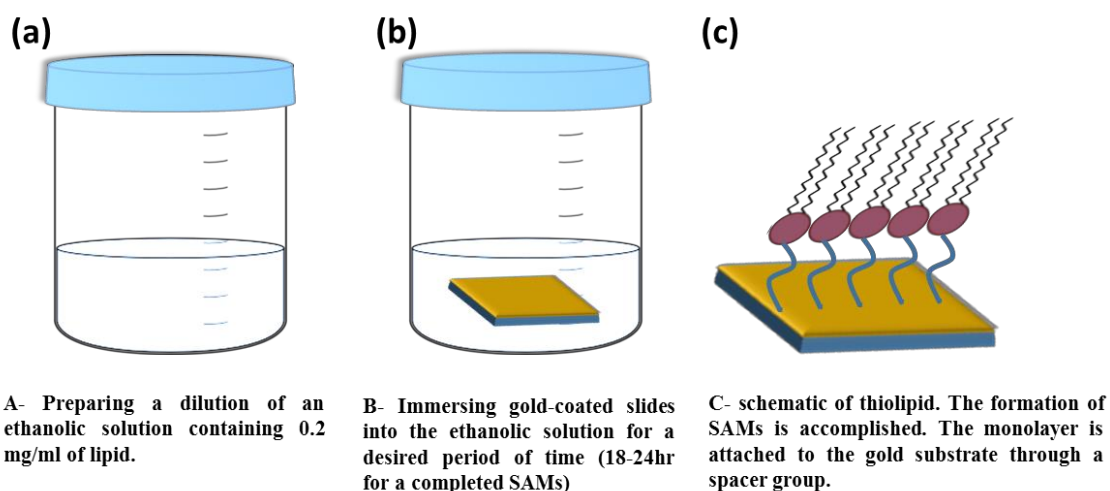
Figure 7: Procedures of Self-assembled Monolayers (SAMs) preparation. This procedure was used to prepare SAMs of DPTL, DDT and 11-MUA.

time. Different types of lipid monolayers have been self-assembled in this work. These lipids are 2,3-di-O-phytanyl-glycerol-1-tetraethylene glycol-D,L-lipoic acid ester lipid (DPhyTL) and two types of alkanethiols (DDT & 11-MUA). For each used thiol, different immersing time of gold substrates has been performed starting from a few minutes up to 24 hours (since 24 hours immersion time leads to a complete and a high quality self-assembled monolayers with no defects and well-ordered monolayers). The effect of the immersion time on the formation of self-assembled monolayers will be examined because the assembly process is considered a time dependent process. After the desired immersion time is completed, the silicon slides were taken out and rinsed thoroughly with ethanol and finally dried under a nitrogen stream (**fig 7**). The monolayers should be completely formed in 12-24 hours of the immersion time. If the immersion time is less than 12 hours, the monolayers are considered as incomplete. Other substrates without the adhesion of self-assembled monolayers are also prepared in order to be used as references. These samples were heated to 400 C° in UHV system for removing adventitious hydrocarbons [11].

4 Chapter 2: Surface Analytical Techniques

A number of surface analytical techniques have been applied in order to investigate the composition and the electronic structure of the samples (11-MUA, DDT and DPhyTL). The investigation of molecular arrangement of the model systems of natural bio-membranes and organic films (alkanethiols) can provide a good understanding of the physical properties of biological membranes. Additionally, these studies are useful in terms of understanding the function and the way in which membranes function. All the investigations of the samples were carried out in an ultra-high vacuum system (UHV) designed via SPECS (Berlin, Germany) with 10^{-8}-10^{-10} mbar of base pressure [35]. These surface analytical techniques include ion spectroscopy and electron spectroscopy are described below.

4.1 Ion spectroscopy

Ion scattering spectroscopies (ISS) in general use the interaction between ions and matter to get information about the composition and structure of surfaces or top surfaces' layers [36].

4.1.1 Neutral impact collision ion scattering spectroscopy (NICISS)

Neutral Impact Collision Ion Scattering Spectroscopy (NICISS) is employed for investigating the structure of soft matter surfaces. NICISS is used for determining the depth or the thickness of elements with reference to the stopping power that will give information about the structure of soft matter surfaces.
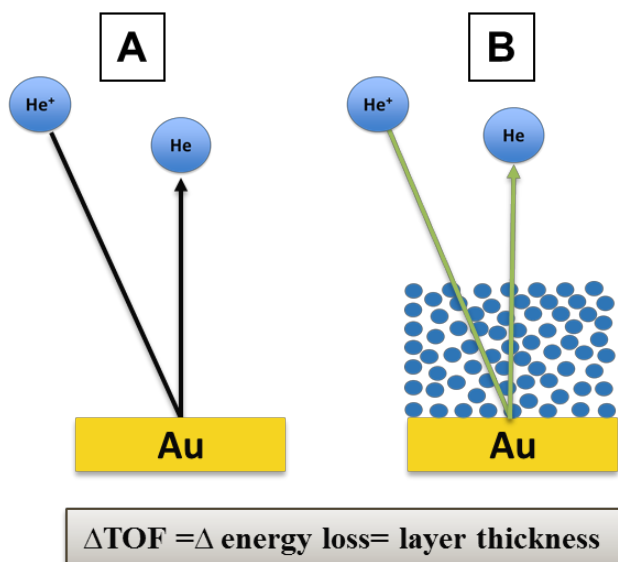
Figure 8: This diagram schematically illustrates the principle of NICIS Spectroscopy. The helium atoms are backscattered from a layer then they will lose energy due to the collision with atoms forming that layer. Difference in TOF measurements from two spectra obtaining from A and B processes gives a difference in energy loss and that leads to estimate the depth of the measured film [36, 37].

NICISS uses inert gas ions such as helium ions (He^+) as projectiles with a primary energy of 3 KeV that can investigate samples in 20-30 nm in depth [36, 37]. Time of flight (TOF) detector is used in NICISS in order to detect neutrals backscattered ions by micro-channel plates under an angle of around 180°. When Helium projectiles are backscattered, energy is lost through the collision of the atoms with the atomic target (**fig 8**). TOF detector measures the distance that the projectiles need to travel from the target to the detector. Therefore, TOF measurements is considered as representation of the amount of energy has been lost during the back scattering process. The energy can be lost in two different ways. The first way through energy loss is due to energy transfer from the ion during collision to the target which is dependent on the mass of the atom being targeted [36, 38]. Energy is hence lost as the ions pass through the target. Second, energy is lost when the target atom experiences electronic excitation and scattering at a small angle. The depth of the atoms, which backscatters projectiles, is identified through this energy loss. The energy loss is continuous as electronic excitation takes place throughout the NICISS process. The loss of energy in the two broad ways leads to the determination of the layer depth [37, 38].

4.2 Electron spectroscopies

Electron spectroscopy or photoelectron spectroscopy is a powerful technique that is capable of determining the composition of samples' surfaces as well the electronic state by analysing the kinetic energy of photoelectron KE of the emitted electrons [39]. The electron needs certain amount of energy to be excited from the initial level to the vacuum level. This amount of energy refers to the binding energy of photoelectron (BE). The binding energy can be determined directly from the measurements whereas the kinetic energy (KE) of the measured photoelectron can be determined by a simple equation:

$$(KE= h\nu\text{-BE })$$

Where $h\nu$ is the excitation energy of the electrons, h represents Planck constant = 6.62×10^{-34} Js and ν represents frequency/Hz of the radiation [39, 40].

4.2.1 X-Ray Photoelectron Spectroscopy (XPS)

X-Ray Photoelectron Spectroscopy XPS is a powerful technique that provides a quantitative analysis of the surface composition [39]. XPS works in the same principle as the MEIS in determination of energy lost in the excitation of molecules as well as the content of a material in terms of depth. In XPS, the absorption of the photon via an atom leads to ionization and emission of a core electron from a core level (**fig 9, 10**). The photoelectric effect explains the phenomenon behind emitting electrons via materials after getting irradiated by photons of sufficient energies, where the KE of an ejected electron can be determined by Albert Einstein's equation:

$$(\text{ KE= } h\nu\text{-BE- } \Phi sp \text{ })$$

Where $h\nu$ refers to the excitation photon energy, and Φsp refers to the spectrometer work function of the detector [41]. Monoenergetic x-rays source (Mg Kα) is used in order to irradiate the samples with excitation energy $h\nu$ =Mg Kα (1253.6eV), where Kα means the electrons transition occurring to produce the X-ray photons. Using soft x-rays with $h\nu$ range between 200 to 2000 eV helps in examining core-levels of samples [39, 42]. The pass energy which is the energy of the analyser was 10 eV. The angle of helium ion beam and X-ray source radiation is 54° as well as the angle of the analyser [35]. X-ray photoelectron spectroscopy gives information about what elements occur in a surface in the range of 20-200 Å and their quantities as well [43]. Additionally, XPS measures the electronic state of elements of samples and from the peak shift, the chemical states of elements of samples can be obtained [39, 44].

Furthermore, the density of electronic states and binding energies can be obtained by applying XPS technique (**fig 9**).

XPS technique is used for the electrons that have escaped into the vacuum of the instrument from the sample after a photon passes through the sample. As the photoelectron travels through the sample, sample reactions such as recombination, inelastic collisions and excitation of the sample occur to the molecules and ions that make up the sample. Various states can also be recaptured and be trapped within the material as the photoelectron moves through
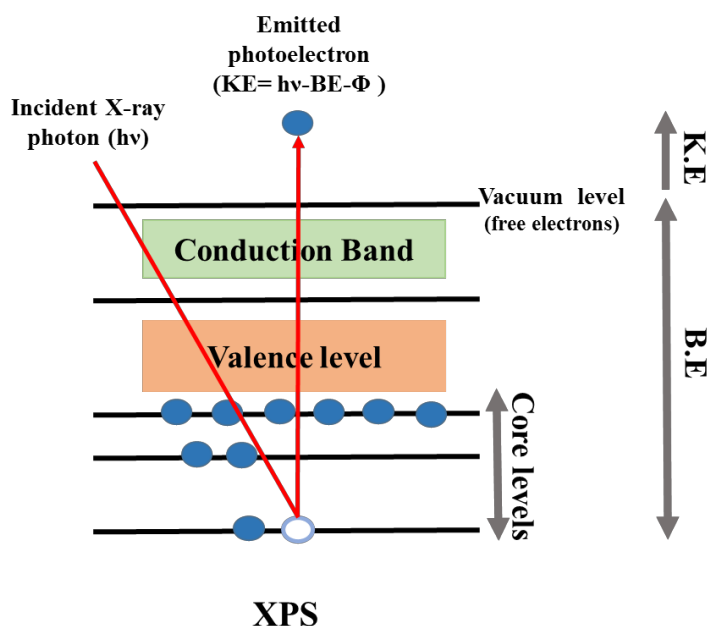
Figure 9: *This diagram schematically illustrates the principle of X-ray photoelectron spectroscopies* [34, 35].

the sample. The process of trapping and recapturing of the states within the material leads to a reduction of the number of photoelectrons that are emitted from the sample through X-ray photoelectron spectroscopy. As the depth increases, the results of photoelectrons emitted appear to attenuate exponentially. The analyses are hence detected by the signals. The surface weighted signal that is exponential is measured by XPS. The depth of the material that has been layered can hence be calculated through X-ray photoelectron spectroscopy [39].
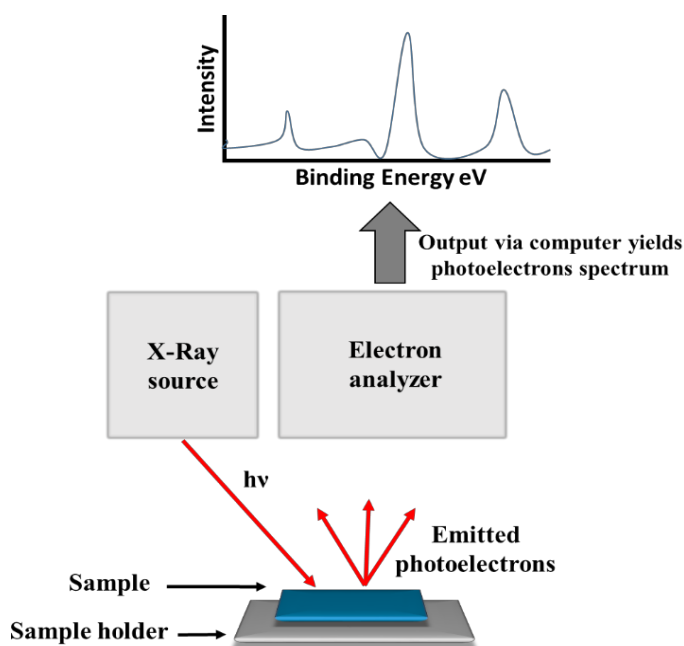
Figure 10*: Schematic diagram of X-ray photoelectron spectroscopy. The sample is positioned on a holder that is electrically in contact with the spectrometer ground. Samples will be irradiated by the X-ray source then electrons will be emitted due to photoelectric effect. The result then is shown as a spectrum of photoelectron intensity as a function of BE* [39].

4.2.2 Angle-Resolved XPS (ARXPS)

Surface sensitivity increases in XPS via varying the angle at which electrons are detected from the surface. If electrons are detected at some angle to the surface normal, the depth information is decreased by an amount equal to cos θ. This method is known as Angle-Resolved XPS [45]. ARXPS is the angle between the surface normal and the emitted electrons .This method often requires tilting samples to a range of angles 0°- 60° with respect to the detector [46, 47]. In this work, a qualitative analysis has been performed on length scale of 3λ [41]. The vertical maximum sampling depth (d) of a solid sample probed by the XPS method is given by: d = 3λ, where λ is the electron inelastic mean free path (in our experiments, the major component of the used thiols is carbon and λ for C =30 Å) [48], and θ is the detection angle measured from the sample surface (ARXPS). The intensity of an element can be calculated by using the following formula:

$$I(d,E,\alpha) = I_0 \exp\left(-\frac{d}{\cos(\alpha)\cdot\lambda(E)}\right)$$

Where I is the intensity, d is the depth (3λ), α is an angle to the surface normal and λ is the probing depth depending on the electron mean free path.
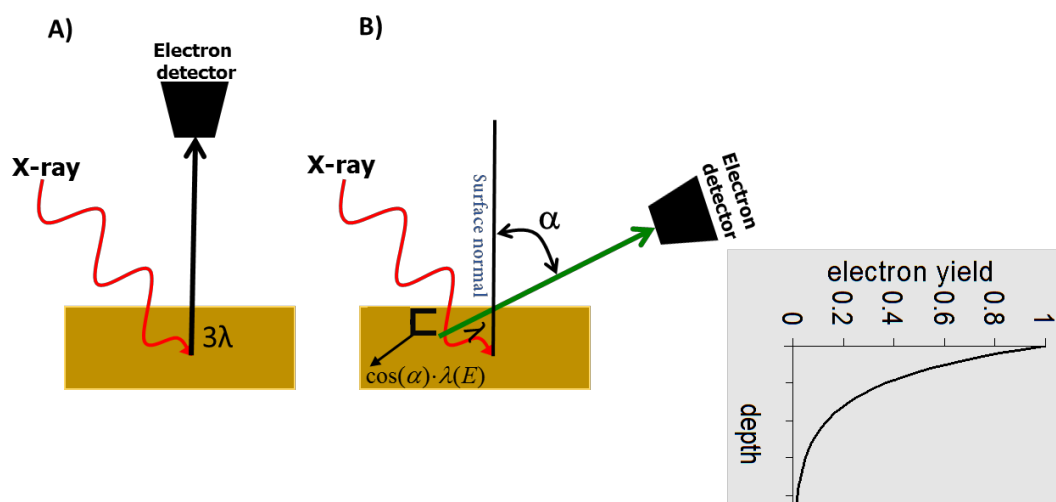
Figure 11: *Illustrates the principle of ARXPS. Tilting the take-off angle of a sample (α) with respect to the detector provides elemental composition over varied sampling depth in XPS.*

A set of measurements over a range of θ gives information about elemental composition over a range of depths. In another words, one can distinguish between the top layer formation elements and the deeper layer by understanding the relationship between the take-off angle and the relative intensity of an element. If intensity increases with increasing angle, element is forming the outer layers and if intensity decreases with decreasing angle, element is forming the deeper layers. Lastly, if intensity does not have an obvious change with angle of observation, element is in between [49, 50].

4.2.3 Metastable Induced Electron Spectroscopy (MIES)

Metastable Induced Electron Spectroscopy is a powerful technique that is used to measure the energy spectrum of the emitted electrons. MIES applies metastable helium atoms that excite atoms and molecules electronically from surfaces at the outermost layers of surfaces [37, 51]. MIES is a surface sensitive technique that probes only the outermost layer of
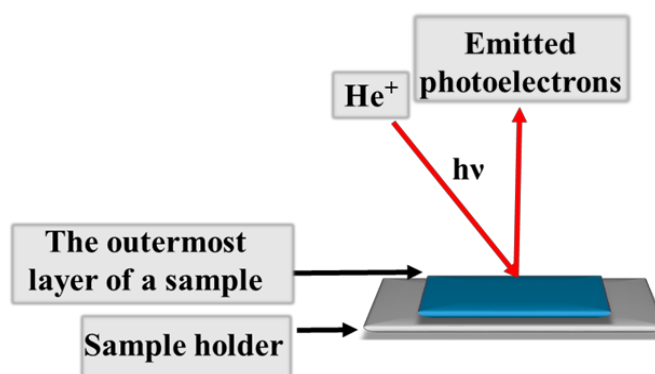
Figure 12: *Schematic diagram of MIES shows metastable helium atoms emitting valence electrons only from the outermost layer of the surface.*

the surface because the interaction of helium atoms with the surface is typically ranged between 0.3 to 0.5 nm [52]. MIES uses metastable helium atoms with an excitation photon energy hv = HeI (19.8eV) [52, 53]. MIES surface sensitivity initiates from the electrons that are on the top layers. The energy spectrum of the emitted electrons, that results from the interaction between the helium atoms and the surface, is measured [53]. The method has various similarities to XPS in some areas. XPS and MIES are both used in the identification of the ion excitation and the determination of the surface content. They both map the electronic structure and the composition of surfaces. However, the techniques are different in terms of what they measure in the material of a solid and more importantly in the surface sensitivity. XPS has higher excitation energy than MIES, thus the exciting radiation of XPS penetrates a few nanometres more into the sample compared to MIES. The mean free path of the ejected electrons determines XPS surface sensitivity. In regards to MIES, the internal excited atoms plays a significant role in reducing the collision-induced damages. In addition, metastable helium atoms are not able to penetrate the material when the material has been excited but rather they release their energy to electrons that are far away from the outermost

layer of the surface [35, 51]. This makes metastable induced electron spectroscopy to a technique that is extremely sensitive to the outermost layer of surfaces (**fig 12**). MIES also has been utilized to examine the outermost electronic structure of several SAMs surfaces such as alkane thiol and carboxylic acid SAMs [54] (**fig 13** [55]) .
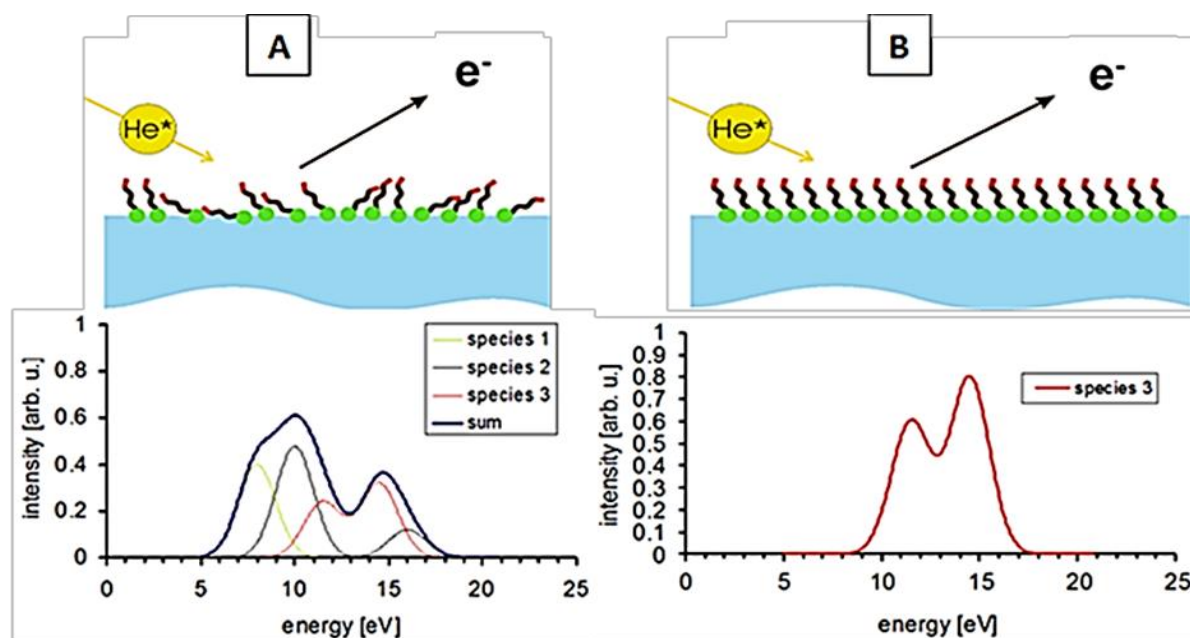
Figure 13: *A) Illustrates helium atoms reaches all parts of the molecules because they are not very ordered and electrons of different orbitals are observed in the spectrum. B) Helium atoms reaches one part of molecules and electrons only of the orbitals forming one side of the molecule can be observed in the spectrum*

5   Chapter 3: Result and discussion

SAMs of thiols provides ordered monolayers when they self-assembled on noble metal surfaces in certain conditions. In this study, different thiols (11-MUA, DDT and DPhyTL) are self-assembled on a gold surfaces in order to determine their properties after they are adsorbed. Additionally, a dilution of SAMs of 0.16mg/ml of DPTL with 0.04mg/ml of mercaptoethanol molecules are prepared as well. Lipids were anchored onto a smooth gold surface because of its property as noble metal as well as the ability of supporting covalent linkages with disulphide and thiol ends of the monolayer [4]. Several surface analytical techniques are employed in this study. The elemental composition and the chemical state of elements occurring on the investigated samples can be investigated by means of XPS while their thickness can be measured by means of NICISS. In addition, the outermost layer composition and the orientation of molecules can be studied by applying MIE spectroscopy.

5.1 NICISS results

SAMs of 11-MUA, DDT and DPhyTL in different immersing times have been examined by means of neutral impact collision ion scattering spectroscopy to determine the thickness of the layer attached to gold. Additionally, a dilution of SAMs of DPTL with mercaptoethanol molecules in different immersing have been examined by means of NICISS. Only the gold coated samples that are used as references, heated to 400 C° before running NICISS measurements for cleaning purposes. Generally speaking, in order to understand the relation between the functionality and the surface structure of self-assembled monolayer and electron-transfer property in particular, it is very important to determine the length of the SAMs [25].
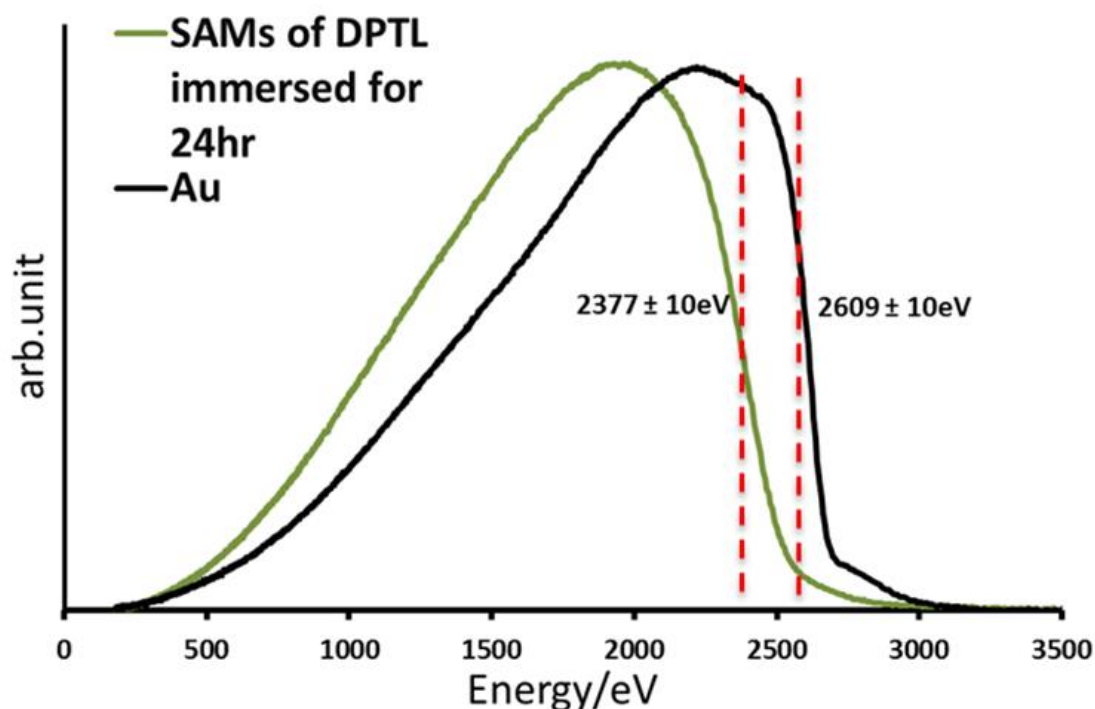
Figure 14: NICISS spectra of gold and gold covered with SAMs of DPTL in 24 hours immersion time.

In order to determine the thickness of the layer attached to the gold surface, the NICIS spectra of the gold surface and the surface that is covered with a self-assembled monolayer are compared. As illustrated in **fig 14**, the onset of the gold NICIS spectrum is compared with NICIS spectrum of the gold surface immersed for 24hr into the DPTL lipid solution. This is chosen as an example because 24hr immersion time is the ideal time for producing a high quality self-assembled monolayers [8]. The principle of NICISS is that when the helium ions hit the layer, they will be backscattered from that layer. Then these helium projectiles will lose energy due to the collision with atoms forming the target. The TOF detector measures the distance that the helium atoms need to travel from the target to the detector. Therefore, TOF

measurements represent the amount of energy lose because the longer time the helium atoms travel from the target to the detector, the more collision occurs between He atoms and the target atoms and thus more energy is being lost. This indicates that the difference in TOF means there is a difference in energy loss and from there the depth of the measured layer can be determined [56]. **Figure 14** illustrates an example explaining the process of the data evaluation of the NICISS data that has been used. It can be seen that compare to the gold sample spectra, the spectra onset signal of the covered sample is shifted to lower energies around 232 ±10 eV. It means the He ions had to penetrate through a longer depth of the sample thus they lost more energy. Now we need to determine the depth or thickness of the investigated SAMs. In order to determine the depth, we need to take the difference between the spectrum without a long range order lose energy during the back scattering process and the spectrum attenuated by small angle scattering which are(nuclear stopping power) and electronic excitations (electronic stopping power), during their trajectory in the matter. For helium ions we used here, the stopping power is equal to 6 eV/Å [56]. Then By determining the energy difference between these two spectra with respect to the stopping power of helium ions, the depth of the investigated SAMs can be evaluated.

We know from the discussion of **fig 14** that the spectra of the substrate covered with SAMs of DPTL which have been immersed for 24hr is shifted to lower energies compare to the uncovered substrate. This gives rise to the following question. Investigating DPTL SAMs with different immersion time, would the spectra of these samples get shifted to lower or higher energies compared to the DPTL SAMs in 24hr of the immersion time? According to previous studies, it is known that the SAMs reach their complete formation within 24hr of the immersion time. Less immersion time than 24hr the monolayers are considered as incomplete. This gives an indication that if the immersion time is less than 24hr, the monolayers will have short hydrophobic alkane chains. Thus, the length or the thickness of these SAMs will be thinner than the thickness of a sample that is immersed for 24hr [8]. This actually can be seen clearly in **fig 15A, B and C** as it illustrates the energy spectra of 11-MUA, DDT and DPTL monolayers, respectively, that have been self-assembled on a gold-coated substrate in a number of different immersion time. The higher the immersing time is, the more spectra onset signal is shifted to lower energies compared to other spectra with lower immersion time. This confirms that there is an effect of the immersing time on the formation of the monolayers. The longer the immersion time is, the thicker the monolayers are (**table 3, 4 and 5**). However, immersing the substrate for more than 24 hours was not recommended because it leads to the

formation of undetermined multilayer structures therefore, the immersion time beyond 24hr were not prepared [4]. I t can be seen in **fig 15D**, which is about the formation of SAMs of 0.16 mg/ml DPTL+ 0.04 mg/ml ME, that the majority of the monolayers' thickness decreases when the immersing time increases. Twenty-four hours immersing time gives a layer length about 1 nm whereas in 5 mins immersing time the length of the monolayer was approximately 3 nm with ± 0.1 nm of uncertainty (**table 6**). To fully understand the reason behind the decrease in the layer thickness, we should see the results obtained from the other applied techniques.

Table 3: *Data obtained from NICIS spectroscopy shows the measured thickness of SAMs of DPTL thiol /nm in five different immersing time/mins.*

Immersing time (mins)	5	15	30	60	1440
Estimated thickness of SAMs of DPTL (nm) with ±0.1 nm uncertainty	2.3	2.6	2.7	3.2	3.9

Table 4: *Data obtained from NICIS spectroscopy shows the measured thickness of SAMs of 11-MUA alkanethiol/nm in three different immersing time/mins.*

Immersing time (mins)	15	30	1440
Estimated thickness of SAMs of 11-MUA (nm) with ±0.1 nm uncertainty	0.7	0.8	1.5

Table 5: *Data obtained from NICIS spectroscopy shows the measured thickness of SAMs of DDT alkanethiol/nm in four different immersing time/mins.*

Immersing time (mins)	1	20	60	1440
Estimated thickness of SAMs of DDT (nm) with ±0.1 nm uncertainty	1	1.2	1.3	1.5

Table 6: *Data obtained from NICIS spectroscopy shows the measured thickness (nm) of a dilution of SAMs of 0.16mg/ml of DPTL with 0.04mg/ml of mercaptoethanol molecules in five different immersing time/mins.*

Immersing time (mins)	5	15	30	60	1440
Estimated thickness of SAMs of a dilution of DPTL with ME (nm) with ± 0.1 nm uncertainty	3	2.9	3.4	1.6	1
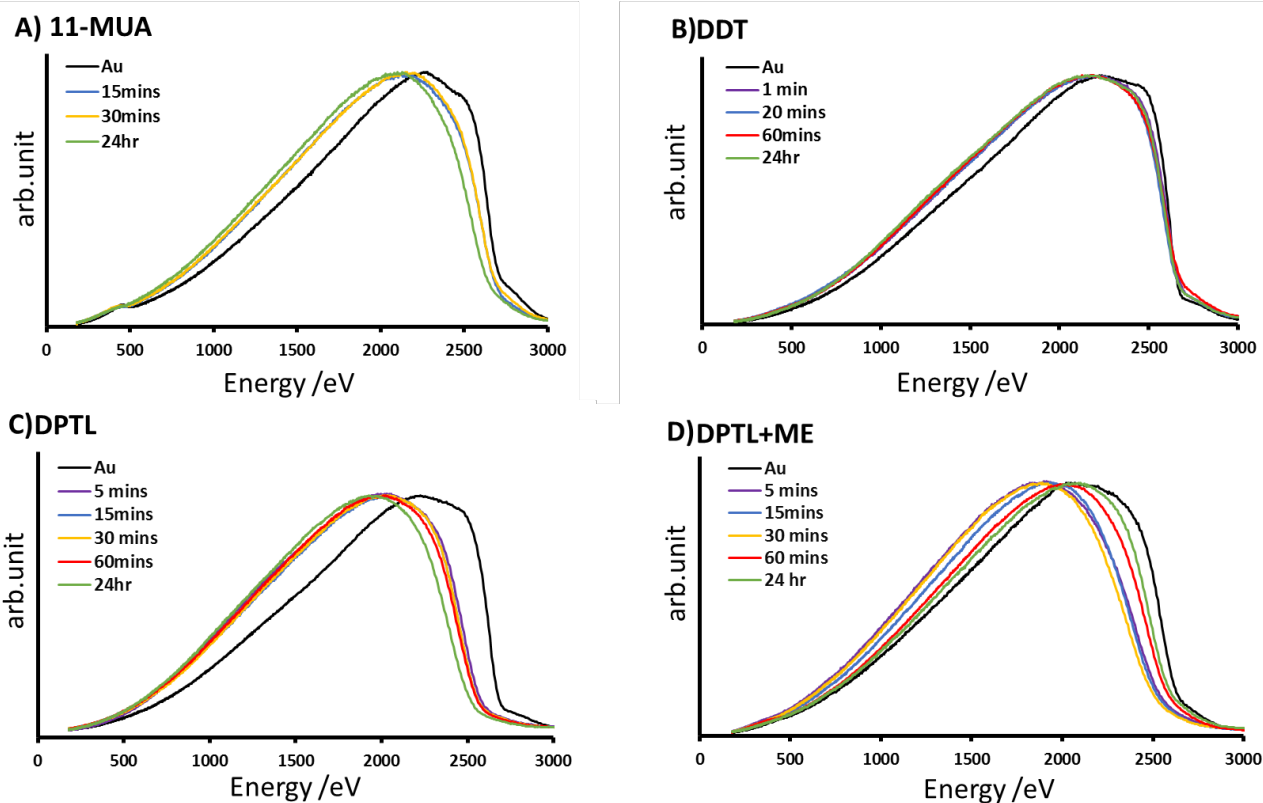
Figure 15: *Shows NICISS results, **A)** Energy spectra of 11-MUA monolayers self-assembled on a gold-coated silicon substrate in three different immersing time 15 mins, 30 mins, and 24 hours including the gold spectrum which was heated up to 400C°. **B)** Energy spectra of DDT monolayers self-assembled on a gold-coated silicon substrate in four different immersing time 1 mins, 20 mins, 60mins and 24 hours including the gold spectrum which was heated up to 400C°. The third spectra **C)** shows the energy spectra of DPhyTL monolayers self-assembled on a gold-coated silicon substrate in five different immersing time 5 mins, 15 mins, 30 mins, 60 mins and 24 hours including the gold spectrum which was heated up to 400C° whereas **D)** shows the energy spectra of a dilution of 0.16mg/ml of DPTL with 0.04mg/ml of mercaptoethanol molecules self-assembled monolayers on a gold-coated silicon substrate in five different immersing time including the gold spectrum which was heated up to 400C°.*

X-ray photoelectron spectroscopy results and discussion

11-MUA, DDT, DPhyTL and a dilution of DPTL with ME monolayers have been self-assembled on a gold-coated substrate at different immersion time and are analyzed by using XPS to determine the atomic and chemical composition of elements forming the samples as well as the relative intensities of each element [35]. CasaXPS software has been used in order to process and fit all the obtained XPS data. High resolution XPS spectra of the core elements presented on SAMs of DPTL and SAMs of DDT are plotted below in fig 16 and 17, respectively, whereas the XPS results for 11-MUA and DPTL+ Me can be found in the Appendix section.

5.1.1 DPTL XPS results
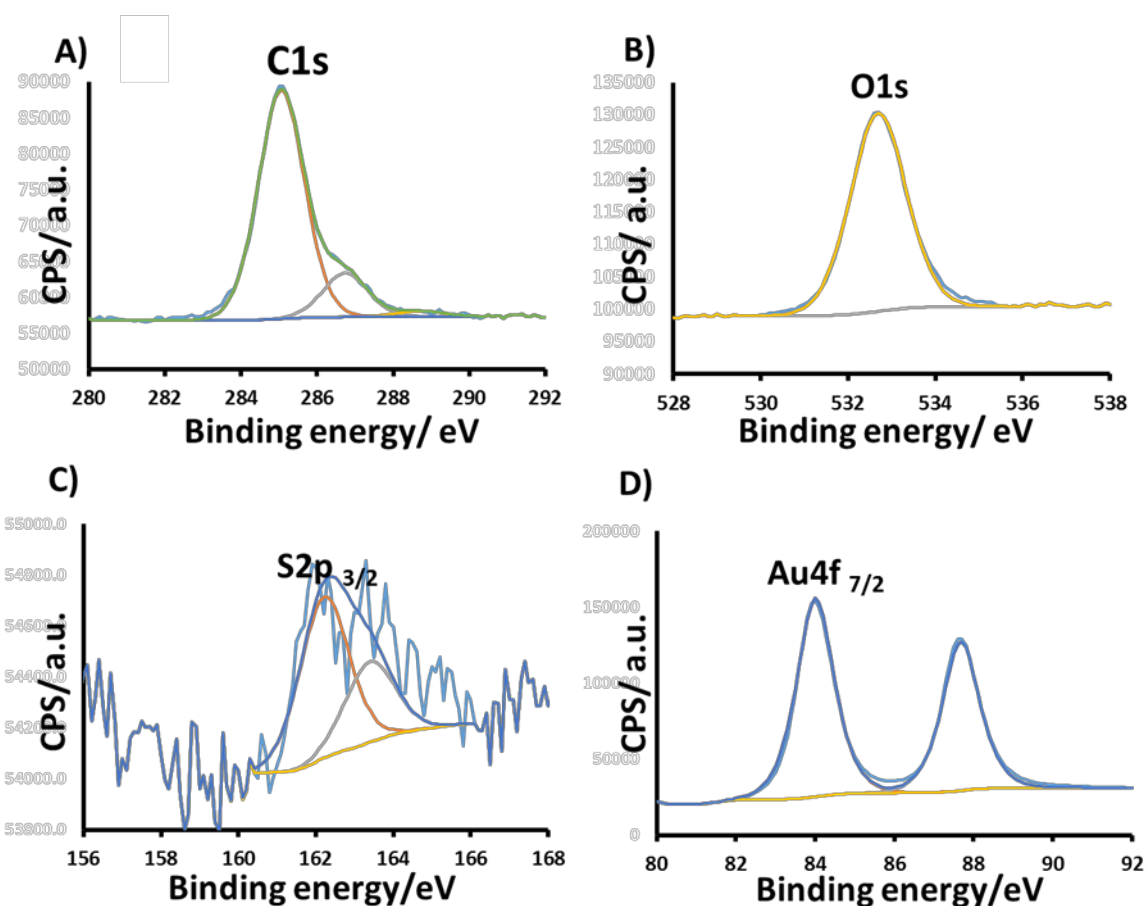
Figure 16: *High resolution XPS spectra of the core elements occur on the SAMs of DPhyTL on gold/silicon substrate (immersed for 24 hours in ethanol solution).* ***A)*** *Illustrates the XPS high resolution spectrum of the C1s region. Three components are required to fit the data accurately. The largest contribution at 285 eV, the other contribution at 286.74 eV and finally the weak contribution at 288.8 eV.* ***B)*** *Shows the XPS high resolution spectrum of the O1s peak at 532.6 eV.* ***C)*** *Displays the XPS high resolution scan of the Sulphur S2p region. One doublet is observed at 162.2eV ($S2p_{3/2}$) and 163.4 eV ($S2p_{1/2}$).* ***D)*** *Shows the XPS high resolution scan of the two doublets with the Au 4f components appeared at a binding energy of 84 eV ($Au4f_{7/2}$) and 87.6 eV ($Au4f_{5/2}$).*

An overall XPS spectrum of the SAMs of DPhyTL anchored on gold/silicon substrate that have been immersed for 24 hours in ethanol solution containing 0.2 mg/ml of lipids, shows the elements C, O, Au and S which represents the elemental composition of DPhyTL ($C_{59}H_{117}O_8S_2$). **Fig 16** shows the peaks for only the core elements forming DPTL anchorlipid and the total XPS result of DPTL elemental composition can be seen in **table 7** below. The number of scans are 8, 10, 10 and 25 for the observed elements Au, O, C and S respectively. **Fig 16A** shows the XPS high resolution spectrum of the C1s signal. Three components are required to fit the data accurately. The energy scale is calibrated with the main carbon peak at 285 ±0.1 eV. The main C peak which is the largest contribution at 285 ±0.1 eV comes from the carbon 1s (C-C), the other contribution at 286.7 ±0.2 eV can be attributed to ether (-C-O-

C-). Finally, as reported in several papers, the weak contribution at 288.89 eV can be attributed to carboxyl (O=C-OH) [57, 58]. **Fig 16B** shows the XPS high resolution spectrum of the Oxygen 1s signal. The component of the O1s peak appearing around 532.6 ±0.1 eV is shown to contain a contribution of single bonded oxygen in phosphate groups (PO, PO-), C–OH, and/or C–O–C [46]. **Fig 16C** displays the XPS high resolution scan of the Sulphur S2p signal. The important of sulphur signal in XPS is that it provides information about the degree to which the SAMs are immobilized and gives more information about S–Au bond [59]. One doublet at 162.2 ±0.2 eV (S2p$_{3/2}$) and 163.4 ±0.2 eV (S2p$_{1/2}$) is observed with the S2p components with an intensity ratio of 2:1. The former has been assigned to thiolate sulphur (covalently bounded to the gold surface) which gives a clear indication that thiols has occured on the gold substrate [46, 47]. The latter might correspond to the unbound (thiol) forms or might be attributed to sulphide component [48, 50]. **Fig 16D** shows the XPS high resolution scan of gold Au 4f region. In the case of well-ordered SAMs (24 hours self-assembled monolayers), one observes two doublets with the Au 4f components appeared at a binding energy of 84 ±0.1 eV (Au4f$_{7/2}$) and 87.6 ±0.2 eV (Au4f $_{5/2}$) as expected. This indicates that the deposited film is indeed metallic gold [46-48]. The conclusion that can be driven from XPS results is that the elemental composition for SAMs of DPTL shows the presence of sulphur, carbon, oxygen, gold which confirms that SAMs are successfully immobilized on Au substrates.

Table 7: Data obtained from XPS illustrating the obtained values of peak positions/eV and the relative intensities/ 100% of the elements presented in the SAMs of DPhyTL anchored on gold/ silicon substrate that have been immersed for (0, 5, 15, 30, 60 and 1440 mins) in ethanol solution containing 0.2 mg/ml of DPhyTL lipid.

Immersing Time Elements		0 mins	5 mins	15 mins	30 mins	60 mins	24 hours
C	**Peak position** **B.E/eV (±0.2eV)**	284 285.5	285.2 286.8 288.9	285 286.5 288.7	285 286.5	285 286.5 288.3	285 286.7 288.7
	Relative intensity % **~ (±5%)**	26.3	66.9	66.2	64.8	61.8	59
O	**Peak position** **B.E/eV (±0.2eV)**	530.5	532.9	532.8	532.8	532.6	532.7
	Relative intensity % **~ (±5%)**	4.1	10.9	9.5	11.6	15.7	20.5
S	**Peak position** **B.E/eV (±0.2eV)**	_	162.2 163.1	162.2 163.3	162.1 163.3	162.2 163.4	162.2 163.3
	Relative intensity % **~ (±5%)**	_	1	1	0.9	0.7	0.6
Au	**Peak position** **B.E/eV (±0.2eV)**	84 88.6	84 87.4	84 87.6	84 87.6	84 87.6	84 87.6
	Relative intensity % **~ (±5%)**	67.5	21	22.6	22.6	18.8	13.8
Si	**Peak position** **B.E/eV (±0.2eV)**	_	_	_	_	102	102
	Relative intensity % **~ (±5%)**	_	_	_	_	2.8	5.8
Ti	**Peak position** **B.E/eV (±0.2eV)**	459.4 466	_	459	_	_	_
	Relative intensity % **~ (±5%)**	2	_	0.4	_	_	_

From **table 7**, mainly it can be concluded that an increase of the immersion time comes along with an increase of the carbon and sulphur peak relative intensities and a decrease of the oxygen and gold peak relative intensities [60]. The appearance of Si element in both 60 mins and 24 hr immersion time, and Ti element in 0 and 15 mins immersion time, might be caused by these samples being scratched during the preparation procedure. This explanation justifies the very low peak intensities of Si and Si elements.

5.1.2 DDT XPS results
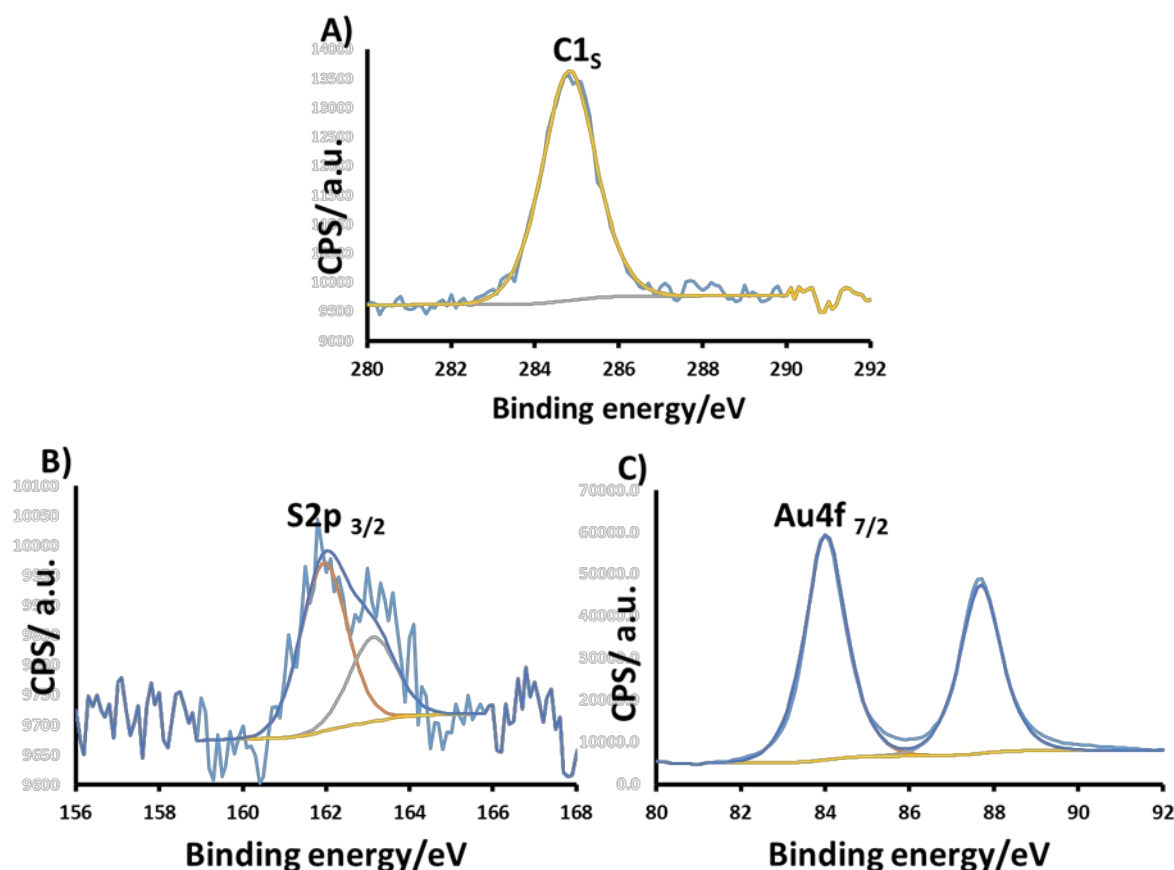
Figure 17: *High resolution XPS spectra of the core elements occur on the SAMs of DDT on gold/silicon substrate (immersed for 24 hours in ethanol solution). **A)** Illustrates the XPS high resolution spectrum of the C1s region. One component observed at a binding energy 284.9 eV is required to fit the data accurately. **B)** Displays the XPS high resolution scan of the Sulphur S2p region. One doublet is observed at 162eV (S2p3/2) and 163.3eV (S2p1/2). **C)** Shows the XPS high resolution scan of the two doublets with the Au 4f components appeared at a binding energy of 84 eV (Au4f7/2) and 87.8eV (Au4f 5/2).*

An overall XPS spectrum of the SAMs of DDT anchored on gold/silicon substrate that have been immersed for 24 hours in ethanol solution containing 0.2 mg/ml of lipids, shows the elements C, S and Au which represents the elemental composition of DDT ($C_{12}H_{26}S$). **Fig17A** shows the XPS high resolution spectrum of the C1s signal. One component is required to fit the data accurately. The energy scale is calibrated with the main Carbon peak at 285 ±0.1 eV. The main C peak in DDT SAMs is observed at 284.9±0.1 eV and it comes from the core level of carbon 1s (C-C). **Fig 17B** displays the XPS high resolution scan of the Sulphur S2p signal. One doublet at 162 ±0.2 eV (S2p3/2) and 163.3 ±0.2 eV (S2p1/2) is observed with the S2p components with an intensity ratio of 2:1. The former has been assigned to thiolate sulphur that is covalently bounded to the gold surface while the latter

might correspond to the unbound thiols or sulphide component. In short, the XPS spectra of the DDT SAMs confirmed that carbon, sulphur and gold were the only atoms present.

Table 8: *Data obtained from XPS illustrating the obtained values of peak positions/eV and the relative intensities/ 100% of the elements presented in the SAMs of DDT anchored on gold/ silicon substrate that have been immersed for (0, 1, 20, 60 and 1440 mins) in ethanol solution containing 0.2 mg/ml of DDT alkanethiol.*

Immersing Time / Elements		0 mins	1 mins	20 mins	60 mins	24 hours
C	**Peak position** B.E/eV (±0.2eV)	284. 285.6	285	284.8	285 286.8 288.6	284.9
	Relative intensity % ~ (±5%)	24.3	53.7	52.4	56	51.5
S	**Peak position** B.E/eV (±0.2eV)	–	162 163.3	162 163.4	162 163.3	162 163.3
	Relative intensity % ~ (±5%)	–	2.2	2	2	2
Au	**Peak position** B.E/eV (±0.2eV)	84 88.6	84 87.7	84 87.8	84 88	84 87.8
	Relative intensity % ~ (±5%)	75.6	44	45.5	41.8	46.4

From **table 8,** it can be seen that the peak relative intensities of S stays constant except for the uncovered sample (gold sample, 0 mins) the intensity of sulphur is zero. The gold sample has approximately 75% intensity of Au element. The carbon and gold intensities do not have a significant change between 1 min to 24 hr of the immersion time. From this table, it can be concluded that the DDT alkanethiols have the ability to bind to the gold substrate within a minute of their immersion time. The SAMs of DDT which has the formula ($C_{12}H_{26}S$) has been formed well in the gold surface without any contaminations.

5.2 DPTL Angle-Resolved XPS (ARXPS) results

In ARXPS measurement, it is possible to obtain very detailed information of the layer ordering, molecular orientation and the relative changes in intensities of elements occur in the surface [26, 61]. Additionally, ARXPS was used to study the spatial distribution and chemical environment of elements in the outermost layer. High resolution spectra have been taken for all elements that form SAMs of DPhyTL lipid. In this work, SAMs of DPhyTL "which has been immersed for 24 hours in ethanol solution containing 0.2 mg/ml of lipids" observed in a series of sample tilt angles (0°, 30°, 45° and 60° with respect to the surface normal).
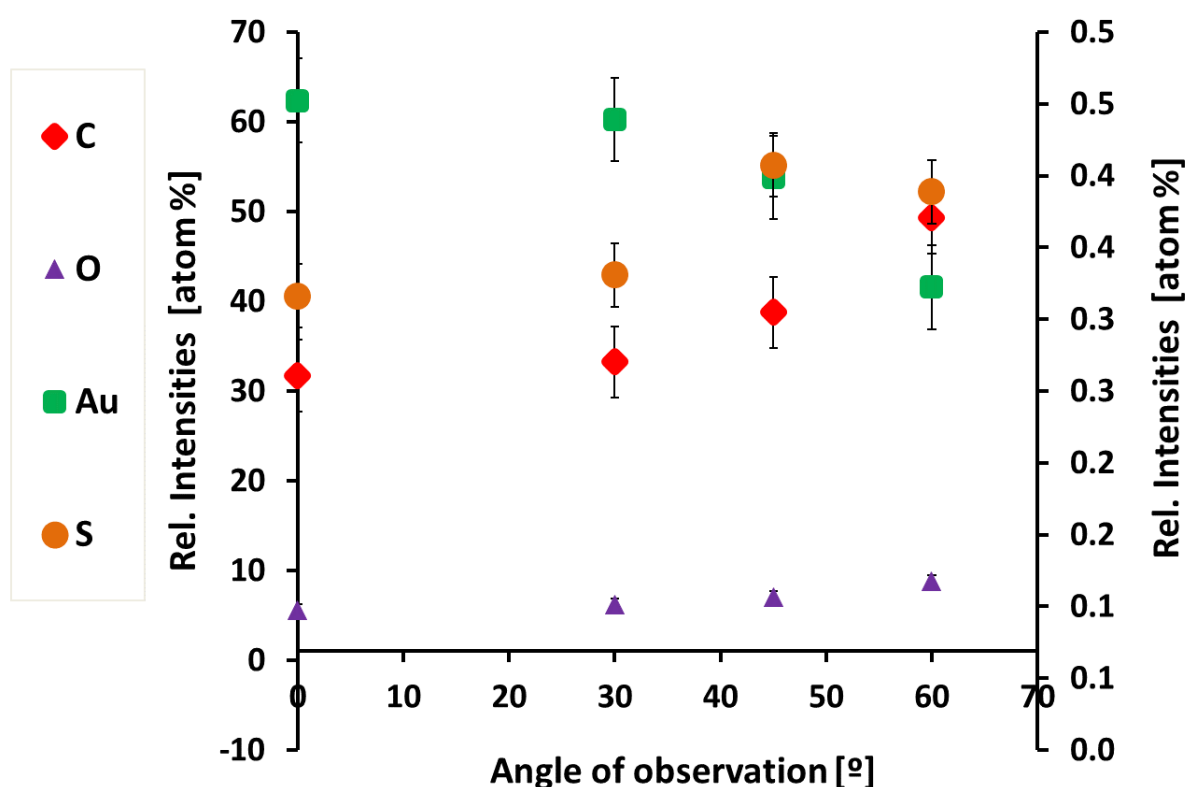
Figure 18: *Illustrates the Atomic intensities of elements present on the SAMs of DPhyTL (immersed for 24 hours in ethanol solution containing 0.2 mg/ml of lipids) observed in four different angle-resolved XPS (0°, 30°, 45° and 60°). The data for S element is plotted to the secondary vertical axis in order to be clear to the reader because S relative intensity is close to zero.*

Fig 18 shows intensities of elements occur on the SAMs of DPTL (immersed for 24 hours in ethanol solution 0.2 mg/ml) in a range of angles observation. Starting with C, there is an increase of the relative intensity of C with the increment of the angle resolved XPS whereas one can observe a decrease in Au relative intensity with the increment of the angle resolved XPS. This occur because when θ = 0°, electrons have to cross the shortest path to be

detected from the surface. Therefore, by tilting the sample up, electrons will cross longer path and thus the probability of a collision between electrons is increasing which causes the electron to change its direction and thus losses more energy. This says that the dipper an element in the sample, the higher is the likelihood that it loses additional energy and the intensity will decrease. Therefore, if the intensity of a certain element increases with the increase of the ARXPS, it has a tendency to be located more in the outer layer. That actually explains what we see in **fig 18**, the C intensity goes up with the increase of the take-off angle and that means it is forming the outermost layer. In contract, the Au intensity goes down with the increase of the take-off angle and this indicates that the Au layer is forming the deeper layer. This confirms that the carbon layer is located on the top of another layer which is the layer of Au. For the O layer, there is a slight increment of the O intensity with the increment of the take of angle.   In regards to S element, it is an intermediate layer where it rather increases or decreases [49].

5.3 MIES results

MIES is highly sensitive to the composition of the external layer, as well as the orientation of molecules. Therefore, it gives a detailed description about the valence electrons occur at the outermost layer of samples that would help in getting some information of molecular orientation. In order to analyse and evaluate a series of MIES spectra, a mathematical algorithm known as singular value decomposition (SVD) is applied. A detailed description of SVD can be found in ref [62]. However, here a brief description of SVD algorithm is given. Generally speaking, In MIES spectra, if samples are prepared and measured under similar conditions, SVD reproduces these measured MIE spectra as a linear combination of reference spectra [62, 63]. In the present work, a number of samples have been prepared and measured by means of MIES under similar conditions (different immersion time). Often the reference spectra in MIES experiment are not known. Therefore, SVD is required to be applied in order to determine the number of reference spectra that are required to reconstruct the set of the measured MIES spectra. Additionally, the SVD procedure results in a set of base spectra that are not necessarily have a physical meaning (e.g. negative intensities) due to the mathematical procedure that they came from. The base spectra can be any linear combination of the reference spectra. After that, the actual reference spectra must be determined in another separate procedure [35, 64] and [62].

In the present study, the procedure of Morgner et al. has been followed. For forming the matrix, we must multiply the base spectra with a (n×n) matrix where n refers to how many base spectra exist. All elements of the diagonal matrix (n×n) are chosen such that two criteria are met (the all elements are singular values). The two main criterion that must be followed in defining matrix elements are:

1. All reference spectra must have non-negative intensities. All measured spectra must be fitted with a linear combination of the reference spectra [35].

$$S_i = \sum_n a_n S_n^r$$

Where: Si refers to the measured spectra, S_n^r refers to the reference spectra and a_n refers to the weighting coefficients.

2. The sum of all weighting coefficients factors must have a physical meaning. In another words, they must be equal to one or close to unity [35, 62].
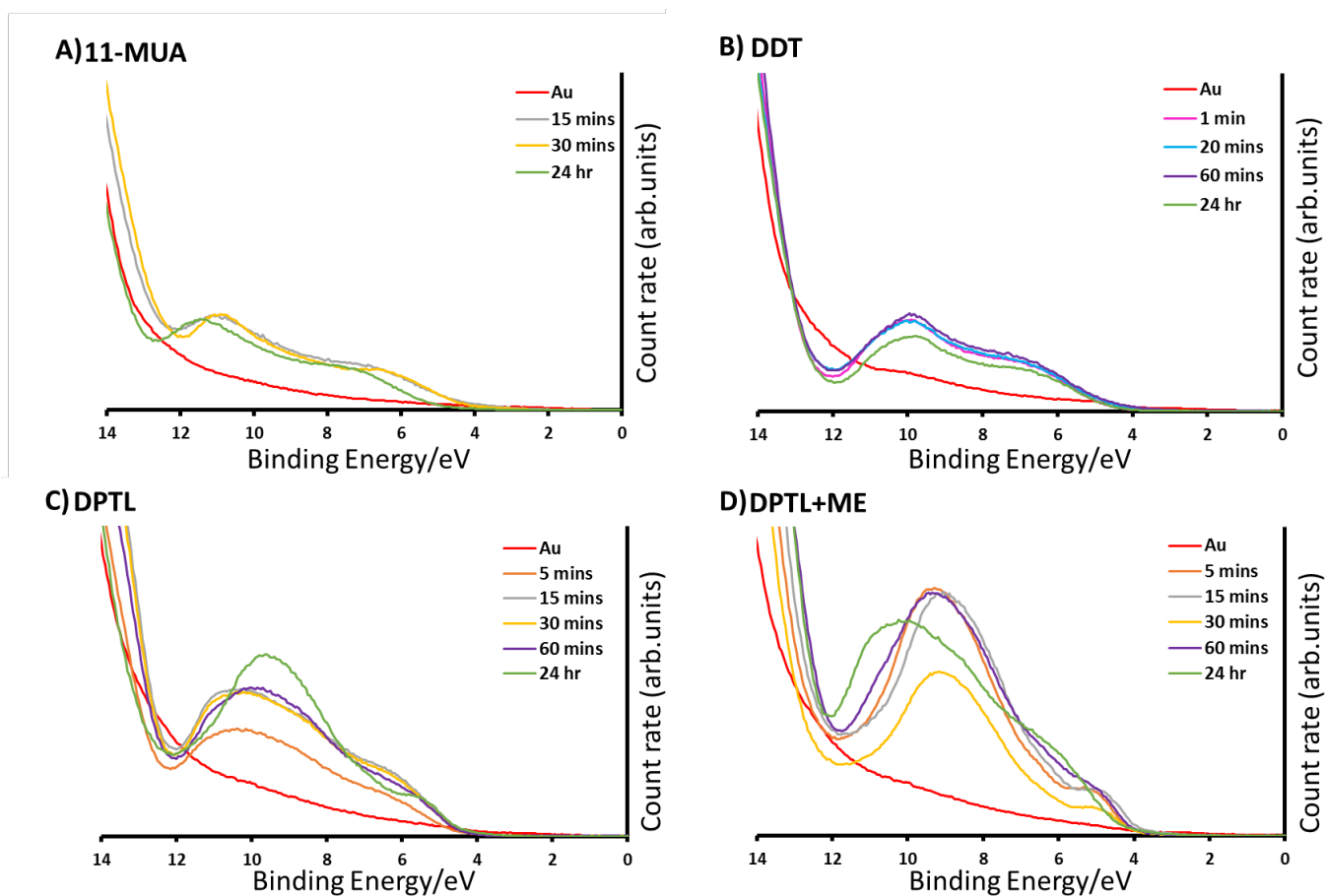
Figure 19: *Data obtained from MIES **A)** shows electron binding energy spectra of SAMs of 11-MUA on gold/silicon substrate in three different immersing time. **B)** Shows electron binding energy spectra of SAMs of DDT on gold/silicon substrate in four different immersing time. **C)** Shows electron binding energy spectra of SAMs of DPTL on gold/silicon substrate in five different immersing time. Lastly, **D)** shows electron binding energy spectra of a dilution of 0.16mg/ml of DPTL with 0.04mg/ml of mercaptoethanol molecules self-assembled monolayers on a gold-coated silicon substrate in five different immersing time.*

MIES data has been taken as a measure for the top surface elemental composition. The result of MIES spectra for SAMs of all investigated thiols 11-MUA, DDT, DPTL and a dilution of DPTL with ME in different immersing time are illustrated in **fig 19A, B, C and D**. For MIES data analysis and evaluation, singular value decomposition (SVD) algorithm has been applied. Therefore, the MIES spectra in **fig 19A, B, C and D** can be reconstructed with a number of reference spectra that shown below in **fig 20A, 21A, 22A and 23A** respectively. These reference spectra could fit the set of the measured spectra shown in **fig 19**. Reference spectra in SVD algorithm gives peaks that are representation of certain functional groups. A separate description of SVD results of each investigated thiol (e.g. 11-MUA, DDT, DPTL and a dilution of SAMs of DPTL with ME) is given below where reference1, 2, 3 and 4 spectra are attributed to weighting factor 1, 2, 3 and 4 spectra, respectively.

5.3.1 MIES discussion for 11-MUA
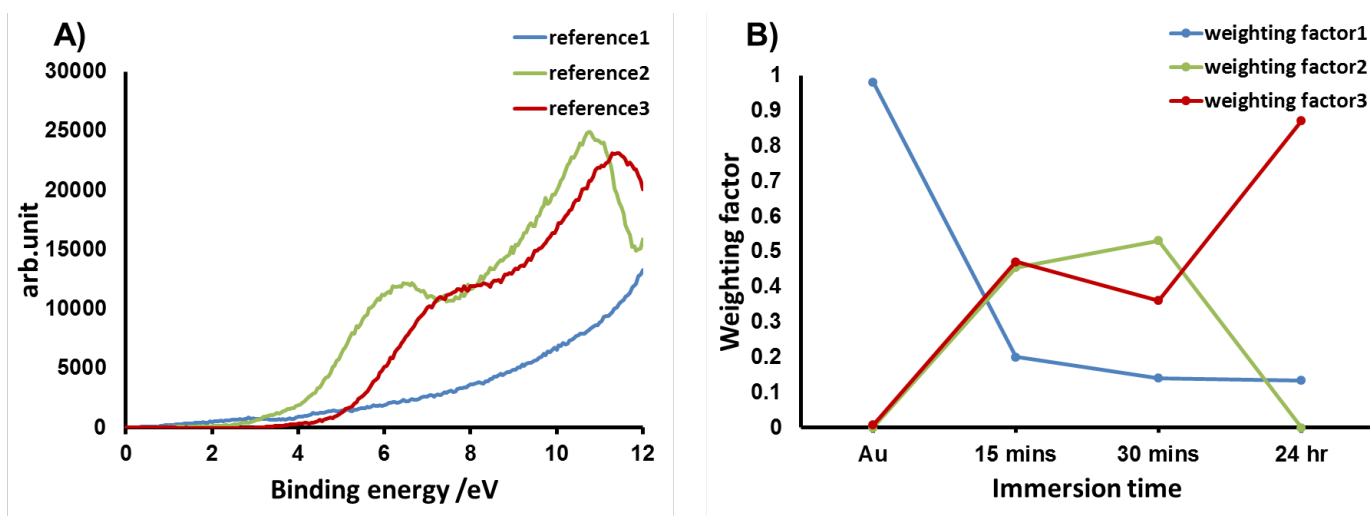
Figure 20: *A) Illustrate reference spectra 1, 2 and 3 that used for fitting the set of MIES spectra shown in fig 16A. **B)** MIES weighting factors for fitting the measured spectra SAMs of 11-MUA on gold/silicon substrate with the reference spectra.*

For 11-MUA SAMs on gold/silicon substrate in three different immersion time including Au spectrum, three reference spectra (**fig 20A**) could fit the measured MIES spectra of 11-MUA SAMs shown in **fig 19A**. From **fig 20B**, three spectra were resulted from the fitting procedure and they indicate that there are three independent components forming the SAMs of 11-MUA. In **fig 20B**, weighting factor 1 ,which is attributed to reference 1 that has sort of a featureless spectrum is attributed to gold layer, decreases with the increment of the immersion time because the Au layer has covered with another layer. The other two spectra, which are very similar in shape, have two peaks each. For reference 2 spectrum, the peaks rising around 7.5 eV and 11.9 eV are referred to the CH_2 group [65]. By looking at the weighting factor 2 one can observe that the CH_2 group are not dominating the surface because the weighting factor2 is decreasing and the weighting factor 3 is dominating the surface. Our assumption of the reference 3 component is that it might be attributed to the terminated group of 11-MUA molecules which is carboxylic acid (COOH) because the weighting factor 3 is increasing with the increase of the immersion time. It is known that SAMs orient themselves spontaneously and become highly ordered and oriented when they are immersed for 24hr [8]. That means the weighting factor which is dominating the outermost layer could be attributed to the terminated group of 11-MUA which is carboxylic acid. To be more precise with that we would later compare the obtained result with computer calculations (Gaussian calculations) of the molecular orbitals because that would give a more reasonable identification of the peaks of the spectra.

5.3.2 MIES discussion for DDT
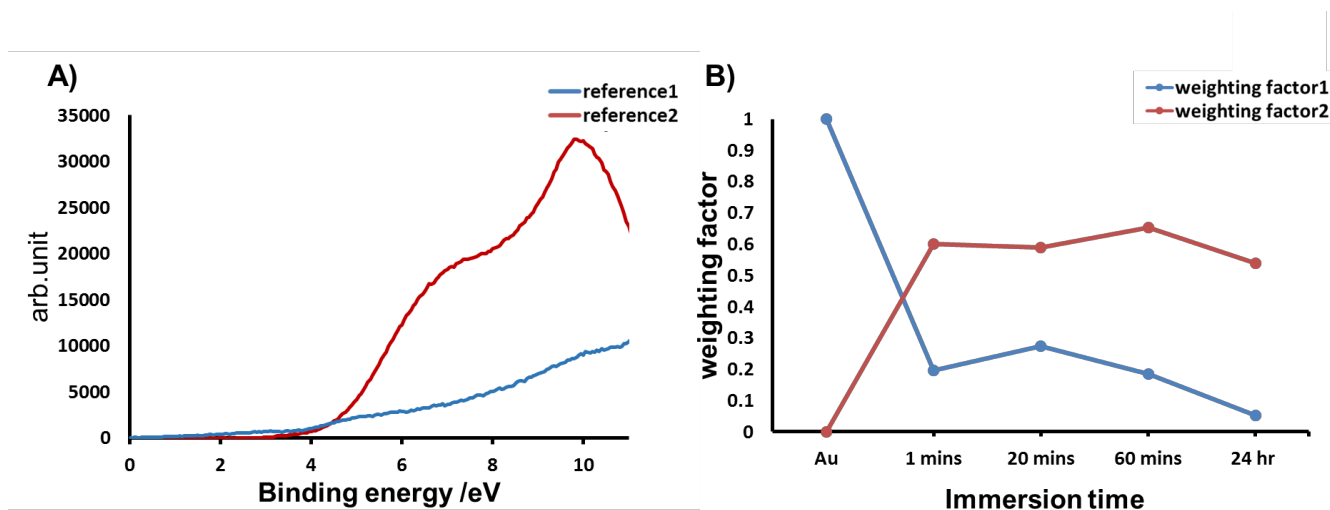
Figure 21: A) *Illustrate reference spectra 1, 2 and 3 that used for fitting the set of MIES spectra shown in fig 16B.* ***B)*** *MIES weighting factors for fitting the measured spectra SAMs of DDT on gold/silicon substrate with the reference spectra.*

Regarding to DDT SAMs on gold/silicon substrate in four different immersion time including Au spectrum, two reference spectra (**fig 21A**) could fit the measured MIES spectra of DDT SAMs shown in **fig 19B**. The two reference spectra in **fig 21A** indicate that there are two independent components forming the SAMs of DDT ($C_{12}H_{26}S$). Reference 1 is sort of an artefact because it has sort of a featureless spectrum that might represent the Au layer because in **fig 21B** the weighting factor 1 shows a rapid decrease from 0 to 1 minute of the immersion time. That means another layer has started to cover the gold layer. Reference2 spectrum has two peaks rising around 10eV and 13eV. These peaks can be attributed to the methyl group (CH_3) which terminate the DDT alkanethiol [28].

5.3.3 MIES discussion for DPTL
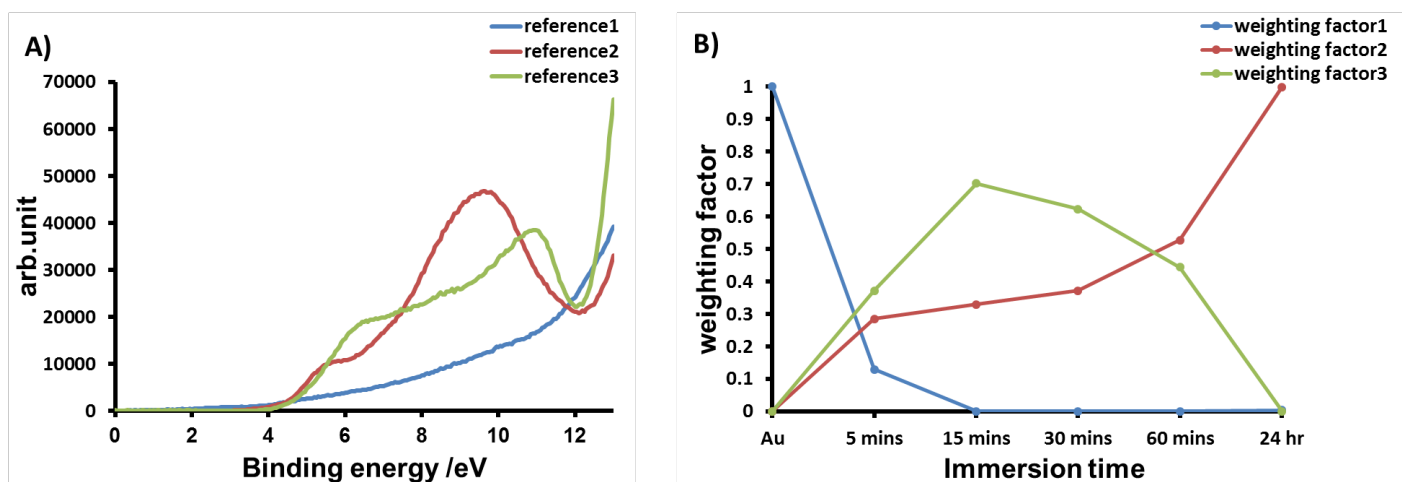
***Figure 22:** A) Illustrate reference spectra 1, 2 and 3 that used for fitting the set of MIES spectra shown in fig 16C. **B)** MIES weighting factors for fitting the measured spectra SAMs of DPTL on gold/silicon substrate with the reference spectra.*

For DPTL SAMs on gold/silicon substrate in five different immersion time including Au spectrum, three reference spectra (**fig 22A**) could fit the measured MIES spectra of DPTL SAMs shown in **fig 19C**. **Fig 22A** indicates that there are three independent components forming the SAMs of DPTL. There are various ways for analysing the reference spectra that were used for the fitting procedure of the set of MIES spectra. One way is comparing the shape of the reference spectra with the shape of existing spectra that have been analysed in previous studies. In **fig 22A**, Reference 1 spectrum, which has sort of a featureless spectrum, might be attributed to a pure element (gold) as the weighting factor 1 was dominating the surface at the beginning and started to decrease with the increase of the immersion time. Which means that another layer is progressing to cover the Au layer. The other two spectra have two peaks each. For the reference 2 spectrum, the peaks rising around 5.2 eV and 9.8 eV are referred to CH_3 standing molecules according to Heinz and Morgner [28]. From **fig 22B**, it can be seen that weighting factor 2, which is attributed to reference spectrum 2, is gradually increasing with the increase of the immersion time whereas weighting factor 3 is decreasing. That means the outermost layer is dominated by the CH_3 group of DPTL which have long chain thiols. This indicates that the SAMs are highly ordered and oriented. According to Heinz and Morgner study, the shape of reference 3 is attributed to lying flat molecules. The two rising peaks in reference3 that are shifted to higher energy at 4.6 eV and 8.7 eV, compared to reference 2, indicates that the CH_2 molecules are dominating the top layer of DPTL thiol in the first 30 mins of the immersion time before starting to drop [28].

5.3.4 MIES discussion for DPTL+ME
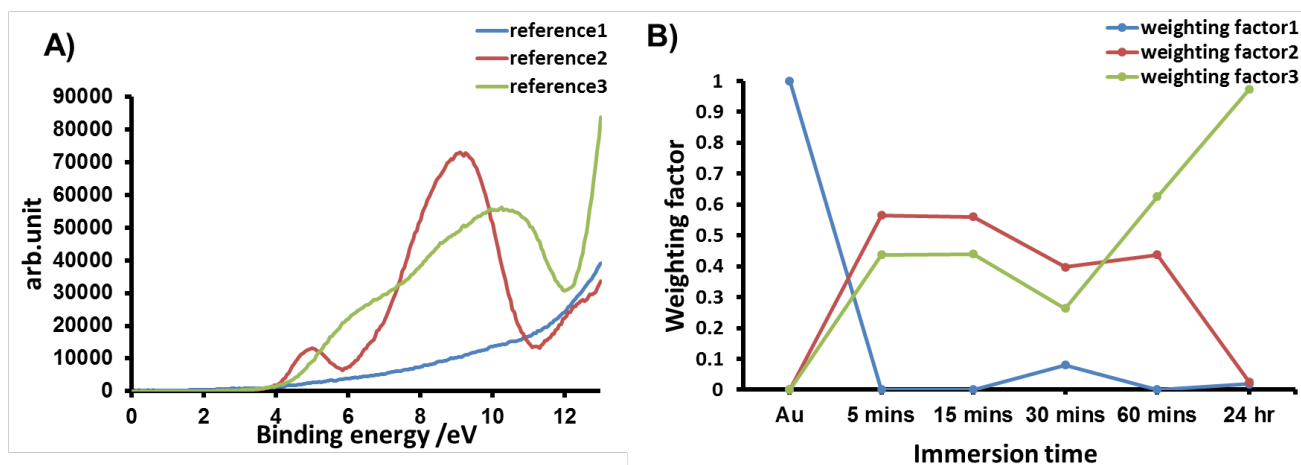
***Figure 23:** A) Illustrate reference spectra 1, 2 and 3 that used for fitting the set of MIES spectra shown in fig 16D. **B)** MIES weighting factors for fitting the measured spectra of the SAMs of a dilution of DPTL with ME on gold/silicon substrate with the reference spectra.*

Fig 23A shows three reference spectra that could fit the measured MIES spectra of the SAMs of a dilution of DPTL with ME shown in **fig 19D**. The three reference spectra indicate that there are three independent components forming the SAMs of DPTL+ME. Reference 1 might be attributed to gold layer as we explained earlier in **fig 22**. The shape of reference 2 and 3 in **fig 23A** resembles the shape of reference 2 and 3 in **fig 22A**, respectively. Therefore, it can be said that reference 2 in **fig 23A** refers to CH_3 standing molecules whereas reference 3 attributes to CH_2 molecules lying flat [28]. From **fig 23B**, it can be seen that weighting factor 3, which is attributed to reference spectrum 3, is dominating the outermost layer. That means CH_2 group is dominating the outermost layer of the dilution of DPTL with ME. This demonstrates that the SAMs of DPTL are not highly ordered but rather the non-polar chains of the monolayers are oriented towards each other. Our interpretation of the CH_2 group dominating the top layer of SAMs of DPTL with ME is that ME molecules create rooms among the spacer group segments. These rooms cause the hydrocarbons tails to bend towards each other. This describes the reason behind the appearance of CH_2 group in the top layer as concluded from the weighting factors of MIES data of DPTL+ME SAMs. The interpretation of MIES data can explain the decrease in the layer thickness of SAMs of DPTL+ME immersed for 24 hr in the data obtained from NICISS. Diluting DPTL molecules with ME molecules will decrease the density of the monolayer as ME separates DPTL molecules from each other and causes hydrophobic tails to bend towards each other and thus leads to reduction in the layer's thickness [6]. However, in order to have a better understanding of the

monolayers arrangement in the dilution of DPTL with ME molecules, this experiment needs to be repeated with the same concentration of the DPTL and ME molecular weight and also with other concentration values. To be more precise with that we would later compare all the obtained results from MIES with computer calculations (Gaussian calculations) because that would give a more reasonable identification of the peaks of the spectra.

6 Chapter 4:

6.1 Conclusion

DPTL anchorlipid was self-assembled on gold substrate in an absolute ethanol solution containing 0.2mg/ml of lipid. SAMs of DPTL in different immersion time have been examined in terms of their thickness, elemental composition and orientation of the molecules forming the SAMs by means of NICISS, XPS and MIES, respectively. SAMs of DPTL structure were compared with the structure (e.g. length, elemental composition and orientation) of the diluted SAMs of 0.16mg/ml of DPTL with 0.04mg/ml of ME in different immersion time. The overall outcomes of DPTL shows that the longer the immersion time, the thicker the layer becomes and the more oriented and stood up the molecules become. In contrast, a diluted DPTL with ME firstly shows an increase of the layer thickness with the increase of the immersion time. However, the layer thickness decreases towards longer immersion times and was found to be thinnest after the longest immersion time investigated. The orientation of the molecules forming the SAMs of DPTL+ME was found to be lying flat on the surface. Additionally, SAMs of two types of alkanethiols (11-MUA and DDT) have been prepared and analysed in this work. The investigation of the organic films have been performed due to their simple forms that had helped in exploring the way of investigating and analysing the structure of the DPTL anchorlipid. In short, as the chemical nature of the anchorlipids and the spacer-segments can affect the structure of the lipid bilayer membrane, the investigation of DPTL is considered a preliminary step that helps in developing the bilayer structure of the model systems of natural biological cell membrane.

6.2 Future work

For a more comprehensive understanding, it is essential to continue examining and investigating the structure (e.g. the orientation of phospholipids) of DPTL thiolipid in the presence of liquid such as formamide solutions (CH_3NO) and aqueous solutions. The investigation shall be carried out by applying NICISS since it is a vacuum based technique that can investigate samples in solvent molecules. Additionally, different weight

concentrations of diluting DPTL molecules with ME molecules should be investigated in order to study the effect of the ME molar concentrations on the monolayer formation (e.g. thickness and molecular orientation).

7 References

1. Singer, S.J. and G.L. Nicolson, *The fluid mosaic model of the structure of cell membranes.* Science, 1972. **175**(4023): p. 720-731.
2. Nicolson, G.L., *The Fluid—Mosaic Model of Membrane Structure: Still relevant to understanding the structure, function and dynamics of biological membranes after more than 40years.* Biochimica et Biophysica Acta (BBA)-Biomembranes, 2014. **1838**(6): p. 1451-1466.
3. Andrade, J.D., *Surface and Interfacial Aspects of Biomedical Polymers: Volume 1 Surface Chemistry and Physics*. 2012: Springer Science & Business Media.
4. Thet, N.T., *Modified tethered bilayer lipid membranes for detection of pathogenic bacterial toxins and characterization of ion channels*. 2010, University of Bath.
5. Rebaud, S., O. Maniti, and A.P. Girard-Egrot, *Tethered bilayer lipid membranes (tBLMs): interest and applications for biological membrane investigations.* Biochimie, 2014. **107**: p. 135-142.
6. Andersson, J. and I. Köper, *Tethered and polymer supported bilayer lipid membranes: Structure and function.* Membranes, 2016. **6**(2): p. 30.
7. *Lipids, Membranes, and the First Cells*, in *Chapter 6 The Molecules of Life*. p. 99-124.
8. Vockenroth, I.K., *Investigations of tethered bilayer lipid membranes for their potential use in biosensing devices*. 2007, University of Bath (United Kingdom).
9. Andersson, J., et al., *Synthesis and Characterization of Novel Anchorlipids for Tethered Bilayer Lipid Membranes.* Langmuir, 2017. **33**(18): p. 4444-4451.
10. *Lipids*. Phospholipids; Available from: https://courses.lumenlearning.com/boundless-biology/chapter/lipids/.
11. Junghans, A. and I. Köper, *Structural analysis of tethered bilayer lipid membranes.* Langmuir, 2010. **26**(13): p. 11035-11040.
12. Narayanaswamy, S., *Plant cell and tissue culture*. 1994: Tata McGraw-Hill Education.
13. Köper, I., *Insulating tethered bilayer lipid membranes to study membrane proteins.* Molecular BioSystems, 2007. **3**(10): p. 651-657.
14. Sackmann, E., *Supported membranes: scientific and practical applications.* Science-AAAS-Weekly Paper Edition, 1996. **271**(5245): p. 43-48.
15. Castellana, E.T. and P.S. Cremer, *Solid supported lipid bilayers: From biophysical studies to sensor design.* Surface Science Reports, 2006. **61**(10): p. 429-444.
16. Naumann, R., et al., *Tethered lipid bilayers on ultraflat gold surfaces.* Langmuir, 2003. **19**(13): p. 5435-5443.
17. Johnson, S.J., et al., *Structure of an adsorbed dimyristoylphosphatidylcholine bilayer measured with specular reflection of neutrons.* Biophysical journal, 1991. **59**(2): p. 289-294.
18. Ataka, K., S.T. Stripp, and J. Heberle, *Surface-enhanced infrared absorption spectroscopy (SEIRAS) to probe monolayers of membrane proteins.* Biochimica et Biophysica Acta (BBA)-Biomembranes, 2013. **1828**(10): p. 2283-2293.

19.   Schiller, S.M., et al., *Archaea analogue thiolipids for tethered bilayer lipid membranes on ultrasmooth gold surfaces.* Angewandte Chemie International Edition, 2003. **42**(2): p. 208-211.

20.   Becucci, L., et al., *Tethered bilayer lipid micromembranes for single-channel recording: the role of adsorbed and partially fused lipid vesicles.* Physical Chemistry Chemical Physics, 2011. **13**(29): p. 13341-13348.

21.   Shenoy, S., et al., *In-plane homogeneity and lipid dynamics in tethered bilayer lipid membranes (tBLMs).* Soft matter, 2010. **6**(6): p. 1263-1274.

22.   Kozuch, J., et al., *Combined Electrochemistry and Surface-Enhanced Infrared Absorption Spectroscopy of Gramicidin A Incorporated into Tethered Bilayer Lipid Membranes.* Angewandte Chemie International Edition, 2012. **51**(32): p. 8114-8117.

23.   Kristiansen, K., *Molecular mechanisms of ligand binding, signaling, and regulation within the superfamily of G-protein-coupled receptors: molecular modeling and mutagenesis approaches to receptor structure and function.* Pharmacology & therapeutics, 2004. **103**(1): p. 21-80.

24.   McGillivray, D.J., et al., *Molecular-scale structural and functional characterization of sparsely tethered bilayer lipid membranes.* Biointerphases, 2007. **2**(1): p. 21-33.

25.   Brett, C., et al., *Studies on Self-Assembled Alkanethiol Monolayers Formed at Applied Potential on Polycrystalline Gold Electrodes.* Electroanalysis, 2003. **15**(5-6): p. 557-565.

26.   Kondo, T., et al., *Determination of thickness of a self-assembled monolayer of dodecanethiol on Au (111) by angle-resolved X-ray photoelectron spectroscopy.* Langmuir, 1998. **14**(19): p. 5656-5658.

27.   Guidelli, R., *Bioelectrochemistry of Biomembranes and Biomimetic Membranes*. 2016: John Wiley & Sons.

28.   Heinz, B. and H. Morgner, *MIES investigation of alkanethiol monolayers self-assembled on Au (111) and Ag (111) surfaces.* Surface science, 1997. **372**(1-3): p. 100-116.

29.   Kim, J., *Investigations of Thiolated Self-Assembled Monolayers on Gold Substrates by FTIR with Specular Reflectance.*

30.   Schilardi, P., O. Azzaroni, and R. Salvarezza, *A novel application of alkanethiol self-assembled monolayers in nanofabrication: Direct molding and replication of patterned conducting masters.* Langmuir, 2001. **17**(9): p. 2748-2752.

31.   Aldrich, S., *Preparing Self-Assembled Monolayers (SAMs) A Step-by-Step Guide for Solution-Based Self-Assembly.* 2006.

32.   Love, J.C., et al., *Self-assembled monolayers of thiolates on metals as a form of nanotechnology.* Chemical reviews, 2005. **105**(4): p. 1103-1170.

33.   Bain, C.D., et al., *Formation of monolayer films by the spontaneous assembly of organic thiols from solution onto gold.* Journal of the American Chemical Society, 1989. **111**(1): p. 321-335.

34.   Vockenroth, I.K., et al., *Stable insulating tethered bilayer lipid membranes.* Biointerphases, 2008. **3**(2): p. FA68-FA73.

35.   Alshehri, N., et al., *Transfer of Ordered Phospholipid Films onto Solid Substrates from a Drained Foam Film.* The Journal of Physical Chemistry C, 2015. **119**(39): p. 22496-22503.

36.   Andersson, G. and H. Morgner, *Impact collision ion scattering spectroscopy (ICISS) and neutral impact collision ion scattering spectroscopy (NICISS) at surfaces of organic liquids.* Surface science, 1998. **405**(1): p. 138-151.

37.   Andersson, G., H. Morgner, and H. Pohl, *Energy-loss straggling of helium projectiles at low kinetic energies: deconvolution of concentration depth profiles of inorganic salt solutes in aqueous solutions.* Physical Review A, 2008. **78**(3): p. 032904.

38.   Ridings, C. and G.G. Andersson, *Deconvolution of NICISS profiles involving elements of similar masses.* Nuclear Instruments and Methods in Physics Research Section B: Beam Interactions with Materials and Atoms, 2014. **340**: p. 63-66.

39.   Verma, H.R., *Atomic and nuclear analytical methods*. 2007: Springer.

40. Jiang, M., *UPS-k: a set partitioning problem with applications in UPS pickup-delivery system.* Information processing letters, 2005. **93**(4): p. 173-175.

41. Seah, M.P. and W. Dench, *Quantitative electron spectroscopy of surfaces: A standard data base for electron inelastic mean free paths in solids.* Surface and interface analysis, 1979. **1**(1): p. 2-11.

42. Sardela, M., *Practical Materials Characterization*. 2014: Springer.

43. Andrade, J.D., *X-ray photoelectron spectroscopy (XPS)*, in *Surface and interfacial aspects of biomedical polymers*. 1985, Springer. p. 105-195.

44. *learn XPS Analysis of Surfaces and Thin Films*. [cited 2017 18/08]; Available from: http://xpssimplified.com/whatisxps.php.

45. Paynter, R., *An ARXPS primer.* Journal of Electron Spectroscopy and Related Phenomena, 2009. **169**(1): p. 1-9.

46. Cumpson, P.J., *Angle-resolved XPS depth-profiling strategies.* Applied surface science, 1999. **144**: p. 16-20.

47. Watts, J.F. and J. Wolstenholme, *An introduction to surface analysis by XPS and AES.* 2003.

48. Laibinis, P.E., C.D. Bain, and G.M. Whitesides, *Attenuation of photoelectrons in monolayers of n-alkanethiols adsorbed on copper, silver, and gold.* The Journal of Physical Chemistry, 1991. **95**(18): p. 7017-7021.

49. *XPS Facilities*. angle-resolved x-ray photoelectron spectroscop; Available from: http://cmem.unm.edu/facilities/xps-facilities-arxps.html.

50. Fadley, C.S., *Angle-resolved x-ray photoelectron spectroscopy.* Progress in Surface Science, 1984. **16**(3): p. 275-388.

51. Read, S.T., *Metastable Induced Electron Spectroscopy of Iron Pentacarbonyl on Gold*. 2015.

52. Wegewitz, L., et al., *Plasma-oxidation of Ge (100) surfaces using dielectric barrier discharge investigated by metastable induced electron spectroscopy, ultraviolet photoelectron spectroscopy, and x-ray photoelectron spectroscopy.* Journal of Applied Physics, 2011. **110**(3): p. 033302.

53. Houssiau, L., et al., *Investigation of Cs surface layer formation in Cs-SIMS with TOF-MEIS and SIMS.* Surface and Interface Analysis, 2014. **46**(S1): p. 22-24.

54. Stultz, J., S. Krischok, and D. Goodman, *Orientation determination of 2-and 4-chlorobenzylmercaptan self-assembled monolayers using metastable impact electron spectroscopy.* Langmuir, 2002. **18**(8): p. 2962-2963.

55. Andersson, G. *Neutral Impact Collision Ion Scattering Spectroscopy (NICISS)*. Available from: http://www.flinders.edu.au/science_engineering/caps/staff-postgrads/info/andersson-g/.

56. Andersson, G. and H. Morgner, *Determining the stopping power of low energy helium in alkanethiolates with Neutral Impact Collision Ion Scattering Spectroscopy (NICISS).* Nuclear Instruments and Methods in Physics Research Section B: Beam Interactions with Materials and Atoms, 1999. **155**(4): p. 357-368.

57. *XPS of Carbon Nanomaterials*. Available from: http://archive.cnx.org/contents/fdddbf98-39ce-4edc-934e-dd1f7477b52b@2/xps-of-carbon-nanomaterials.

58. Xie, F., et al., *Surface structure characterization of nanodiamond thin film for electronic field emission applications.* Journal of Vacuum Science & Technology B: Microelectronics and Nanometer Structures Processing, Measurement, and Phenomena, 2008. **26**(1): p. 102-105.

59. Etorki, A., F. Massoudi, and M. Abuein, *X-Ray Photoelectron Spectroscopy Study of Surface Complexation Between Trace Metal Ions and Self-Assembled Monolayers.* Advanced Science Letters, 2012. **17**(1): p. 87-100.

60. Devillers, S., et al., *1-Dodecanethiol self-assembled monolayers on cobalt.* Langmuir, 2011. **27**(24): p. 14849-14860.

61. Ye, S., et al., *Characterization of self-assembled monolayers of alkanethiol on GaAs surface by contact angle and angle-resolved XPS measurements.* Surface Science, 2003. **529**(1): p. 163-170.

62.   Andersson, G.G., et al., *Phosphine-stabilised Au9 clusters interacting with titania and silica surfaces: The first evidence for the density of states signature of the support-immobilised cluster.* The Journal of chemical physics, 2014. **141**(1): p. 014702.
63.   Oberbrodhage, J., *Determination of a solute electron energy spectrum not accessible experimentally by means of Singular Value Decomposition.* Journal of Electron Spectroscopy and Related Phenomena, 2000. **107**(3): p. 231-238.
64.   Berlich, A., Y.C. Liu, and H. Morgner, *Evaporation of Ni and carbon containing species onto NiO/Ni as case study for metal support catalysts investigated by Metastable Induced Electron Spectroscopy (MIES).* Radiation Physics and Chemistry, 2005. **74**(3): p. 201-209.
65.   Ozaki, H. and Y. Harada, *Penning ionization electron spectroscopy of n-alkane ultrathin films. Molecular orbitals and orientation of molecules.* Journal of the American Chemical Society, 1990. **112**(15): p. 5735-5740.

8 Appendix

Immersing Time / Elements		0 mins	15 mins	30 mins	24 hours
C	Peak position B.E/eV (±0.2eV)	284.2 285.6 287.3	284.8 286.2 289	284.6 285.5 288.8	285 286.3 289.2
	Relative intensity % ~ (±5%)	31.3	50	47.2	54.3
O	Peak position B.E/eV (±0.2eV)	532.2 533.7	532.2 533.7	532 533.5	532.2 534
	Relative intensity % ~ (±5%)	7.7	7.7	7.1	12
S	Peak position B.E/eV (±0.2eV)	–	162 163.3	162 163.7	162 163 164 165
	Relative intensity % ~ (±5%)	–	2	2.1	1.8
Au	Peak position B.E/eV (±0.2eV)	84 88.5	84 87.6	84 88	84 87.6
	Relative intensity % ~ (±5%)	49.3	39.3	43.4	31.7
Cr	Peak position B.E/eV (±0.2eV)	573 583 576 586	–	–	–
	Relative intensity % ~ (±5%)	11.5	–	–	–

Table 9: Data obtained from XPS illustrating the obtained values of peak positions/eV and the relative intensities/100% of the elements presented in the SAMs of 11-MUA anchored on gold/ silicon substrate that have been immersed for (0, 15, 30 and 1440 mins) in ethanol solution containing 0.2 mg/ml of 11-MUA alkanethiol.

From **table 9,** it can be seen that an increase of the immersion time comes along with an increase of the carbon and oxygen peak relative intensities and a decrease of the gold peak relative intensity whereas there is no a significant change in sulphur peak intensities with different immersion time.

Immersing Time ⟍ Elements		0 mins	24 hours
C	**Peak position**	284	285
	B.E/eV (±0.2eV)	285	286
			288
	Relative intensity % ~ (±5%)	56	71.3
O	**Peak position**	530	532
	B.E/eV (±0.2eV)		
	Relative intensity % ~ (±5%)	9.8	13.3
S	**Peak position**	–	162
	B.E/eV (±0.2eV)		163
	Relative intensity % ~ (±5%)	–	1.1
Au	**Peak position**	84	84
	B.E/eV (±0.2eV)	88	87
	Relative intensity % ~ (±5%)	20.8	14.2
Cr	**Peak position**	574	–
	B.E/eV (±0.2eV)	584	
	Relative intensity % ~ (±5%)	13.2	–

Table 10: Data obtained from XPS illustrating the obtained values of peak positions/eV and the relative intensities/ 100% of the elements presented in the SAMs of 0.16 mg/ml DPTL diluted with 0.04mg/ml of ME that anchored on gold/ silicon substrate that have been immersed for (0, and 1440 mins).

From **table 10**, it can be seen that the peak relative intensities of C, O and S increased with the immersion time whereas the Au intensity decreases. Cr intensity is approximately 13% in the gold sample. This indicates that the sample might have got scratched during the preparation procedure.
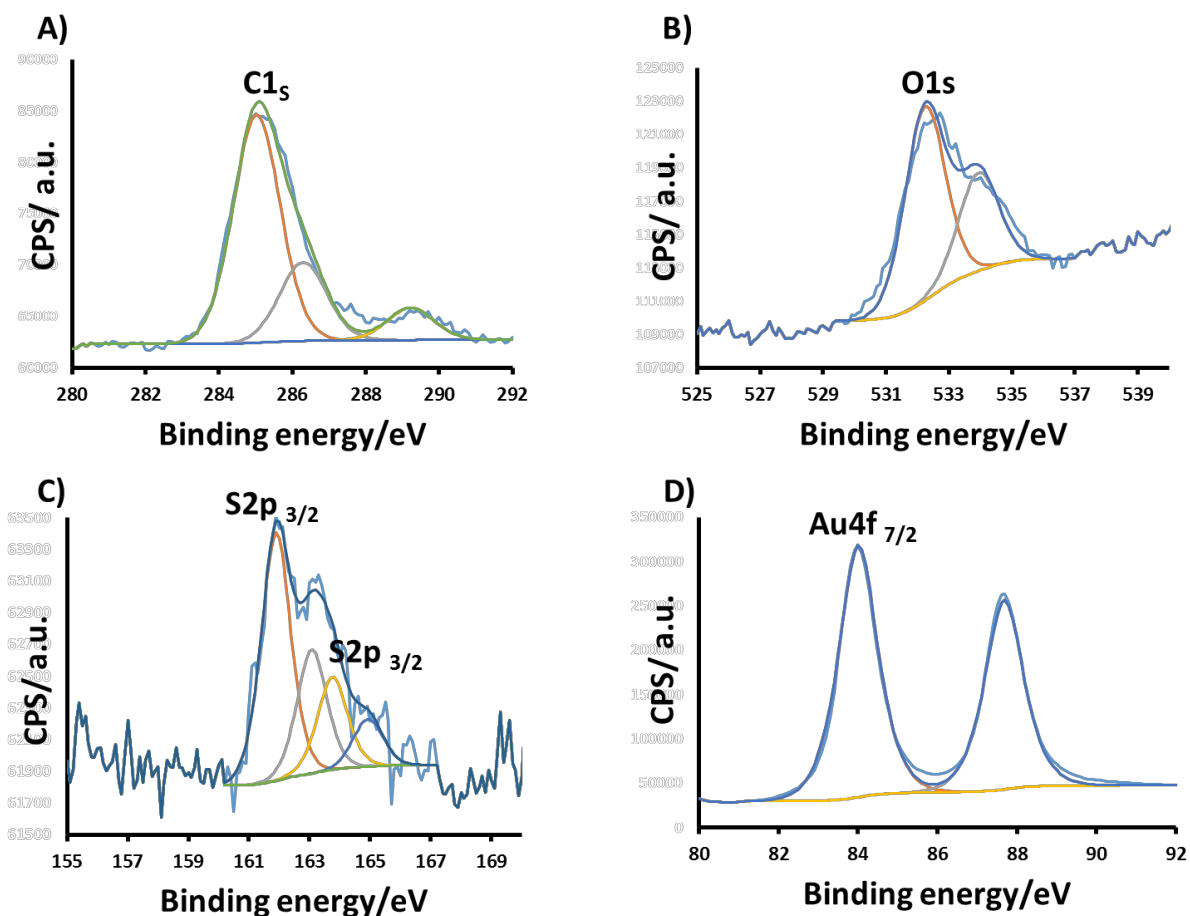
Figure 24: *High resolution XPS spectra of the core elements occur on the SAMs of 11-MUA on gold/silicon substrate (immersed for 24 hours in ethanol solution).* ***A)*** *Illustrates the XPS high resolution spectrum of the C1s region. Three components are required to fit the data accurately. The largest contribution at 285 eV, the other contribution at 286.3 eV and finally the weak contribution at 280.2 eV.* ***B)*** *Shows the XPS high resolution spectrum of the O1s region. Two peaks are observed at 532.2 eV and 534 eV.* ***C)*** *Displays the XPS high resolution scan of the Sulphur S2p region. Two doublets are observed one doublet refers to (S2p3/2) at 162eV and 163 eV and the second doublet refers to (S2p1/2) at 164 eV and 165 eV.* ***D)*** *Shows the XPS high resolution scan of the two doublets with the Au 4f components appeared at a binding energy of 84 eV (Au4f7/2) and 87.6 eV (Au4f 5/2).*

C
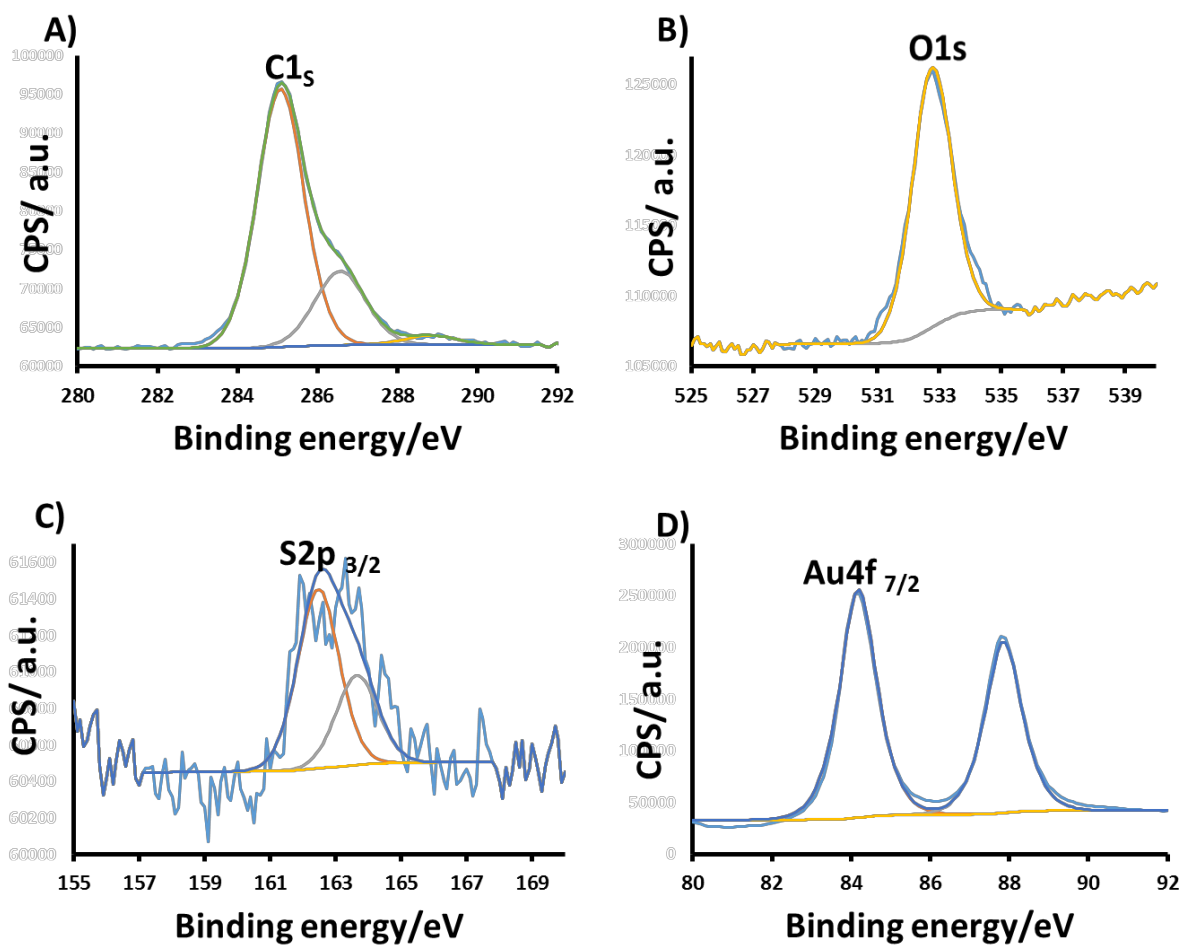
***Figure 25:*** *High resolution XPS spectra of the core elements occur on the SAMs of the diluted 80% DPTL with 20% ME on gold/silicon substrate (immersed for 24 hours in ethanol solution).* ***A)*** *Illustrates the XPS high resolution spectrum of the C1s region. Three components are required to fit the data accurately. The largest contribution at 285 eV, the other contribution at 286.5 eV and finally the weak contribution at 288.8 eV.* ***B)*** *Shows the XPS high resolution spectrum of the O1s peak at 532.7 eV.* ***C)*** *Displays the XPS high resolution scan of the Sulphur S2p region. One doublet is observed at 162.4eV (S2p3/2) and 163.5 eV (S2p1/2).* ***D)*** *Shows the XPS high resolution scan of the two doublets with the Au 4f components appeared at a binding energy of 84 eV (Au4f7/2) and 87.7 eV (Au4f 5/2).*

D